

Step-wise Distribution Alignment Guided Style Prompt Tuning for Source-free Cross-domain Few-shot Learning

Huali Xu, Yongxiang Liu, Li Liu, Shuaifeng Zhi, Shuzhou Sun, Tianpeng Liu, MingMing Cheng

Abstract—Existing cross-domain few-shot learning (CDFSL) methods, which develop training strategies in the source domain to enhance model transferability, face challenges when applied to large-scale pre-trained models (LMs), as their source domains and training strategies are not accessible. Besides, fine-tuning LMs specifically for CDFSL requires substantial computational resources, which limits their practicality.

Therefore, this paper investigates the source-free CDFSL (SF-CDFSL) problem to solve the few-shot learning (FSL) task in target domain with only pre-trained model and a few target samples without accessing source data and training strategy. However, the inaccessibility of source data prevents explicitly reducing the domain gaps between the source and target. To tackle this challenge, this paper proposes a novel approach,

Step-wise Distribution Alignment Guided Style Prompt Tuning (StepSPT), to implicitly narrow the domain gaps from the perspective of prediction distribution optimization. StepSPT initially proposes a style prompt that adjusts the target samples to mirror the expected distribution.

Furthermore, StepSPT tunes the style prompt and classifier by exploring a dual-phase optimization process that combines external and internal processes. In the external process, a step-wise distribution alignment strategy is introduced to tune the proposed style prompt by factorizing the prediction distribution optimization problem into a multi-step simple distribution alignment problem. In the internal process, the classifier is updated via standard cross-entropy loss. Evaluation on 5 datasets illustrates the superiority of StepSPT over existing prompt tuning-based methods and SOTAs. Furthermore, ablation studies and performance analyzes highlight the efficacy of StepSPT. The code will be made public at <https://github.com/xuhuali-mxj/StepSPT>.

Index Terms—Cross-domain few-shot learning, few-shot learning, step-wise distribution alignment, style prompt.

arXiv:2411.10070v1 [cs.CV] 15 Nov 2024

1 INTRODUCTION

CROSS-domain few-shot learning (CDFSL) [1] aims to address the target task with limited data by leveraging a vast dataset from a different domain, *i.e.* source domain. Existing CDFSL methods [2], [3], [4], [5], [6], [7], [8], [9] tackle the target FSL task by utilizing massive data from alternative (source) domains and the corresponding training or adapt strategy, which requests the source data to be accessible and the training strategy can be designed. However, these methods may not always be feasible in real-world scenarios [10] due to the following reasons: (1) The computational burden of training with a large source dataset, particularly for edge devices, poses a significant challenge. (2) Concerns regarding confidentiality, privacy, and copyright may render the source dataset inaccessible. (3) Large-scale pre-training models (LMs) [11], [12], [13], [14], [15], [16], renowned for their robust generalization capabilities, is crucial for CDFSL. Existing methods fail in LMs application scenarios, where source data is inaccessible and training strategy cannot be designed.

To address the above mentioned problems, researchers delve into the exploration of a novel Source-Free CDFSL (SF-

This work was partially supported by National Key Research and Development Program of China No. 2021YFB3100800, the Academy of Finland under grant 331883, Infotech Project FRAGES, the National Natural Science Foundation of China under Grant 62376283 and the Key Stone grant (JS2023-03) of the National University of Defense Technology (NUDT).

Huali Xu and Shuzhou Sun are with the Center for Machine Vision and Signal Analysis (CMVS), University of Oulu, Oulu 90570, Finland (email: huali.xu@oulu.fi; zhuzhou.su@oulu.fi).

Shuaifeng Zhi, Yongxiang Liu, Tianpeng Liu, and Li Liu are with the College of Electronic Science and Technology, National University of Defense Technology, Changsha, 410073, China (email: zhishuaifeng@outlook.com; lilyliu_nudt@163.com).

Corresponding authors: Yongxiang Liu.

Ming-Ming Cheng (cmm@nankai.edu.cn) is with the College of Computer Science, Nankai University, Tianjin, TKLNDST, China.

CDFSL) [17] problem. SF-CDFSL address the FSL task in the target domain exclusively through an existing pretrained model (referred to as the source model), devoid of any access to the source data and training strategy. Figure 1 indicates the differences between the vanilla CDFSL and SF-CDFSL. By relaxing the requirements on accessing source domain data and designing training strategies, the exploring of SF-CDFSL, on the one hand, protects source data privacy, which promote the development of fields with high data privacy requirements, such as medicine [18], [19], remote sensing [20], [21], *etc.* On the other hand, SF-CDFSL can ignore the source data transmission costs [10], [22]. Moreover, the reduced restrictions on training strategy design make it feasible to apply LMs to CDFSL tasks. However, in addition to the challenges inherited from CDFSL, SF-CDFSL has unique challenges [17]: Firstly, in contrast to CDFSL utilizes source and target data, SF-CDFSL relies solely on scarce labeled target data to tackle the FSL challenge, making overfitting easily. Secondly, bridging domain disparities by explicitly aligning source and target distributions becomes unattainable given the unknown of the source data distribution.

To address these challenges, instead of explicitly reducing the gaps between source and target distributions, this paper aims to implicitly reduce these gaps by optimizing the prediction distribution. Using LMs as the source model, we propose Step-wise Distribution Alignment Guided Style Prompt Tuning (StepSPT) to solve the FSL task in the target domain. First, inspired by the ability of batch normalization to adjust style and influence data distribution [23], StepSPT designs a learnable style prompt to reduce the difference between the target and expected distributions, while also constraining the complexity of the hypothesis space. Second, StepSPT utilizes a dual-phase optimization process consisting of external and internal stages.

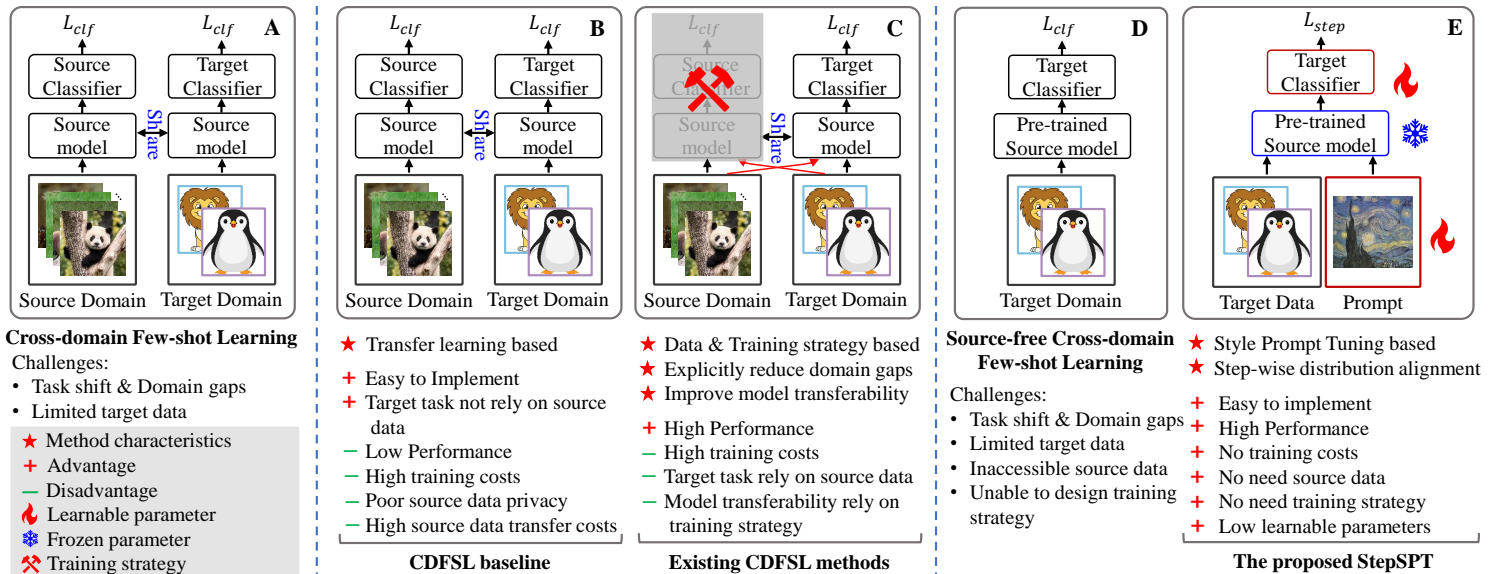


Fig. 1. The difference between CDFSL and SF-CDFSL. **A:** The CDFSL setup. **B & C:** The CDFSL baselines and existing solutions, e.g. introducing the source/target data into the adapt/training process, or exploring the training strategy. **D:** The SF-CDFSL setup. **E:** The proposed StepSPT makes both the pretrained source model and target domain adapt to each other through the learnable style prompt and classifier.

In both phases, the parameters of the LMs remain frozen, while the style prompt and classifier parameters are updated iteratively.

In the external phase, the classifier parameters are frozen, and the transductive learning is introduced to achieve the distribution alignment. Through in-depth analysis of the target domain distribution optimization problem [24], [25], we found that it can be transformed into a multi-step distribution alignment problem. Thus, a step-wise distribution alignment strategy is proposed to optimize the prediction distribution incrementally. This means during the training process, the distribution difference between each two adjacent steps is small. Therefore, this paper gradually reduce the gaps between target and ideal distribution by constraining the domain gap between each two steps. The query set is introduced into the external process. Since the data in the query set are unlabeled, the step-wise distribution alignment strategy uses the data distribution of the previous step as the label and aligns the distribution of the current step to the distribution of the previous step. To ensure the distribution optimization of the subsequent step is not misled by the previous step's distribution during the alignment process, a credible group is formed in the prior step to identify and select trustworthy features for alignment. The prompt learned by multiple alignment steps to make the target distribution gradually approach the ideal distribution. In the internal phase, a standard meta-training strategy is applied to the support set to update the classifier while keeping the prompt parameters fixed. This phase helps the model adapt to the specific characteristics of the target domain. The contributions of this paper are as follows:

- We focus on a new SF-CDFSL problem, and transform the domain alignment challenge between the source and target domains in SF-CDFSL into a target distribution optimization problem. Furthermore, we provide a theoretical analysis and guidance to address this distribution optimization.
- We propose the Step-wise Distribution Alignment Guided Style Prompt Tuning (StepSPT) method to tackle the SF-CDFSL problem. StepSPT introduces a style prompt to adjust the target distribution and employs a dual-phase optimization process including external and

internal stages, where the style prompt and classifier are alternately updated in the external and internal processes. In the external process, we make the target distribution close to the ideal distribution, while let the model adapt to the target FSL task in the internal process. Specifically, in external process, through theoretical analysis, we turn the difficult one-step alignment into simple multi-step alignment. Based on the this, we explore a step-wise distribution alignment strategy to learn the proposed style prompt. Besides, a credible group is introduced to avoid misleading information during alignment, while the traditional cross-entropy loss is used in the internal process to update the classifier.

- Extensive evaluation on 5 datasets indicates the superior performance of the proposed StepSPT, with detailed ablation study illustrating the contribution of each component.

2 RELATED WORK

2.1 Cross-domain Few-shot Learning

Since Guo *et al.* [26] set the BSCD-FSL benchmark and Tseng *et al.* [2] conceptualized it, many studies have appeared in CDFSL [3], [27]. Most of them focused on pre-training strategies in CDFSL [3], [4], [5], [28]. A common practice is to introduce additional data during the training phase to facilitate the acquisition of shared knowledge between the source and the target domain [3], [4], [28], [29]. For example, [3] learns the source domain representation with a self-training strategy by using unlabeled target data. Following the above method, [4] proposes a dynamic distillation-based approach, utilizing unlabeled images from the target domain. Also, [28] uses a small amount of labeled target data for training. They introduced the meta-FDMixup network, which helps the model by mixing up different data and separating important features. In addition, other CDFSL solutions incorporate additional information, such as style, during the pre-training phase [5], [6], [30], [31]. [5] introduces an ISSNet, which enhances model generalization by applying styles from unlabeled data to labeled data. [30] tackle CDFSL by analyzing style variations,

breaking down images into simpler components using wavelet transform to better understand their styles. Furthermore, they also develop a training method called StyleAdv, focusing on meta style adversarial training for CDFSL. Besides, [31] proposes the SET-RCL method, which adapts to new styles by considering both data and model adjustments to mimic the styles of unknown domains. Additionally, [32] introduces a Gia-CFSL framework, combining few-shot learning with domain alignment in hyperspectral image classification through graph information, to bridge the gap between different domains effectively.

Currently, CDFSL technology focus on adaptation strategies in the target domain. This is in addition to in-depth analyses of training strategies in the source domain [8], [9]. [8] use traditional distance-based classifiers and image retrieval views, they apply a reranking procedure to refine the target distance matrix by identifying k-reciprocal neighbors in the task. [9] proposes a dual adaptive representation alignment approach that leverages prototypical feature alignment and normalized distribution alignment to enable fast adaptation of meta-learners with very few-shot samples, leading to SOTA results on multiple benchmarks in the field of few-shot learning. All of these methods have yielded exceptional results, significantly advancing the field of CDFSL. These novel perspectives emphasize the technical potential of exploring the adapt strategy and not relying on the CDFSL training strategy. It is worth noting that all these algorithms require access to source data. In contrast, our SF-CDFSL prevents source data access, eliminating privacy and transmission issues. Furthermore, SF-CDFSL provides a robust method and framework for the application of LMs in CDFSL tasks.

2.2 Source-free Domain Adaptation

The initial foray into Source-Free Domain Adaptation (SFDA) [10] posits that source data is dispensable, advocating for the retention of frozen source classifier parameters to align target representations with source hypotheses' predictions. Subsequently, [33] leverages uncertainty in source model predictions to guide target domain adaptation. Additionally, [34] observes that despite poor performance of the source model in the target domain due to domain gaps, the generated features tend to cluster, prompting the utilization of nearest neighbor methods to minimize distances between similar samples. Some other methods explore the domain-invariant information. For instance, [35] proposes the Domain-Invariant Parameter Exploration (DIPE) method to identify domain-invariant parameters within the source model, thereby enabling the generation of domain-invariant representations. [36] proposes transferring the domain-invariant class relationships to fully leverage the knowledge from the source domain. While some methods solve SFDA through clustering. Specifically, by treating SFDA as an unsupervised clustering problem and leveraging the idea that local neighbors in the feature space are likely to have more similar predictions, [37] proposes optimizing an objective that enforces prediction consistency among neighboring features. [38] constructs a set of semantic class prototypes to cluster target features and assign pseudo-labels, facilitating effective distribution alignment by using these pseudo-labeled target samples along with the class prototypes. Moreover, [39] proposes a Distilling Multimodal Foundation Model (DIFO) approach that maximizes mutual information with the target model using prompt learning, while simultaneously distilling the knowledge model into the target model. Research indicates

that SFDA frequently outperforms conventional Unsupervised Domain Adaptation (UDA) [10]. However, SFDA typically have identical source and target tasks. In contrast, SF-CDFSL encounters domain gaps and task disparities between the source model and the target task, making it more challenging.

2.3 Prompt Learning

Despite the outstanding performance of current large-scale pre-training models (LMs) [11], [12], [13] across a variety of downstream tasks, their massive parameters result in a finetuning process that is both time-consuming and resource-intensive. Therefore, researchers have explored prompt tuning, an efficient approach that fine-tunes a small part of the input prompts instead of all parameters of model. Existing prompt tuning methods [40], [41], [42], [43], [44], [45], [46], [47] typically employ an automated prompt, input alongside data into LMs, to accommodate downstream tasks. Among them, [40], [46] updates a prompt and classifier simultaneously to adjust to the downstream tasks. Furthermore, [41], [42] utilize CLIP as a backbone introduce text prompts, expanding the versatility of prompt tuning. However, due to limited knowledge of target domains, LMs often perform poorly in cross-domain tasks, especially for distant domain. Thus, creating an adaptive prompts for different domains is key to improving LMs' performance in cross-domain tasks.

3 METHODS

3.1 Overview

The primary goal of CDFSL is to address the FSL task in the target domain with the help of source task with sufficient data. Specifically, given a source domain \mathcal{D}^s with task \mathcal{T}^s , and a target domain \mathcal{D}^t with a few-shot learning (FSL) task \mathcal{T}^t ($\mathcal{D}^s \neq \mathcal{D}^t$, $\mathcal{T}^s \cap \mathcal{T}^t = \emptyset$), CDFSL first leverage labeled data from \mathcal{D}^s for solving \mathcal{T}^s . The target domain \mathcal{D}^t includes a support set $S = \{x_i, y_i\}_{i=1}^{N \times K}$ and a query set $Q = \{x_i\}_{i=1}^{m-(N \times K)}$, m means the sample numbers in \mathcal{D}^t . Here, x_i and y_i denote the training samples and their labels in S , forming an N -way K -shot FSL task. The query set Q contains samples from the same N classes as S , used to evaluate the FSL model. The goal of CDFSL is to learn a predictive function f for \mathcal{T}^t using both the limited samples in \mathcal{D}^t and the knowledge from $(\mathcal{D}^s, \mathcal{T}^s)$. The main difference between SF-CDFSL and CDFSL is the accessibility of \mathcal{D}^s . In SF-CDFSL, the source data is inaccessible, and the aim is to address the target FSL task \mathcal{T}^t using only a few labeled data in \mathcal{D}^t and a pretrained source model θ . Existing methods [1], [6], [30], [31] focus on reducing the distance between the source and target domains explicitly. However, these approaches faces two key challenges in SF-CDFSL: (1) SF-CDFSL relies only on limited labeled target data to tackle the FSL task, and (2) explicitly aligning source and target distributions to bridge domain disparities becomes infeasible due to the unknown source data distribution.

In this work, we address the aforementioned challenges by implicitly reducing domain gaps through the optimization of the prediction distribution. Specifically, we propose Step-wise Distribution Alignment guided Style Prompt Tuning (StepSPT) to tackle SF-CDFSL, as illustrated in Figure 2. In Section 3.2, we first explain the motivation behind introducing the style prompt and step-wise distribution alignment. We define prompt tuning in Section 3.2.1 and highlight that existing prompts are not designed for CDFSL. Drawing inspiration from the ability of batch normalization to adjust style and influence data

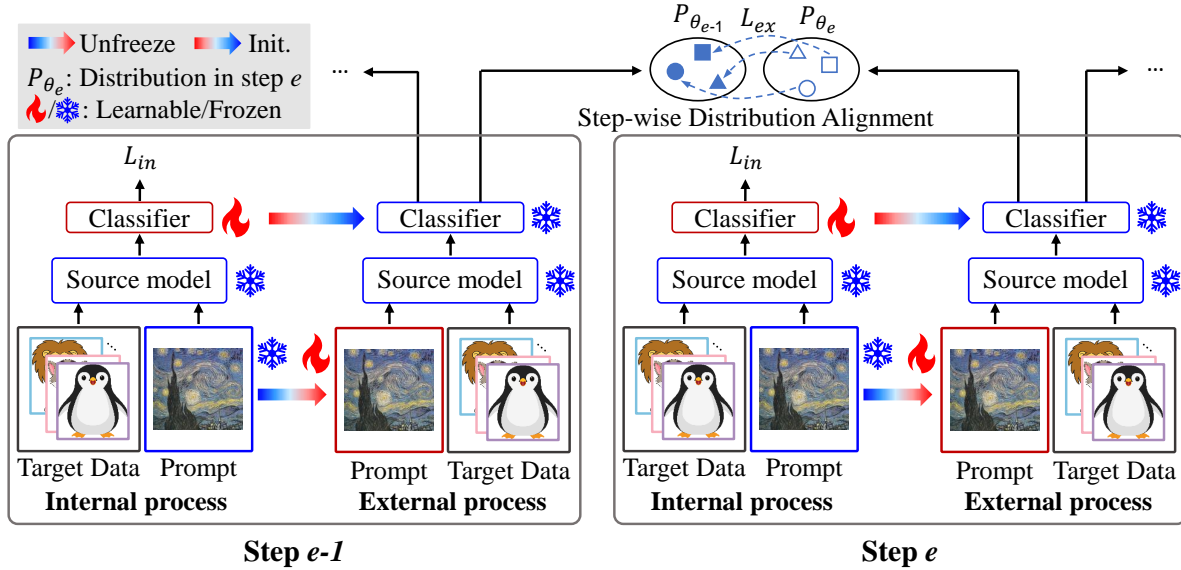


Fig. 2. Overview of StepSPT. In the internal process, only the classifier is updated. In the external process, the proposed style prompt is learned with a step-wise distribution alignment strategy. Between two steps, there can be multiple internal processes. Here, we represent the style prompt with an image format.

distribution [23], StepSPT incorporates a learnable style prompt that modifies data distribution while constraining the complexity of the hypothesis space. Furthermore, in Section 3.2.2, we discuss the challenges of optimizing the target prediction distribution through single-step searching and provide theoretical analysis explaining how step-wise distribution alignment addresses these challenges. Section 3.3 details the proposed method, including the design of the style prompt in Section 3.3.1, the dual-phase optimization process in StepSPT in Section 3.3.2, and a summary of the overall pipeline in Section 3.3.3. Algorithm 1 in Section 3.3.3 outlines the pipeline of StepSPT and summarizes its main operational steps, facilitating a comprehensive understanding of the framework.

3.2 Warm-Up: Why Style Prompt and Step-wise Distribution Alignment?

3.2.1 Why Style Prompt?

Prompt tuning is typically used when the pretrained model is frozen. Based on the descriptions in [48], [49], we define prompt tuning as follows.

Definition 3.2.1. Prompt Tuning. Given a frozen pretrained model θ , a sample space \mathcal{X} , and the corresponding label space \mathcal{Y} , where each input instance $x \in \mathcal{X}$ and each label $y \in \mathcal{Y}$, the goal of prompt tuning is to use a prompting mechanism $f_p(\cdot)$ to modify x into a prompt $x_p = f_p(x)$, such that the model maximizes the likelihood $P_\theta(y|x_p)$ of the correct label y . Here, $f_p(\cdot)$ can be designed either manually by humans or automatically through algorithmic methods.

Take the multi-modal classification task on CLIP [11] as an example. For each image x , a human-designed prompt [48], [49] could be a fixed sentence pattern such as $f_p(x) = "A photo of a [class_x]."$ In contrast, an automatically designed prompt [40], [41], [42] is typically learnable parameters like $f_p(x) = "[V]_1 [V]_2 \dots [V]_M [class_x]"$, where all $[V]$ can be optimized.

Existing automatically designed prompts are not designed for cross-domain scenarios. Inspired by the influence of style on data distribution [23], this paper proposes a style prompt to adjust the target data distribution and mitigate performance degradation caused by cross-domain issues. Additionally, the style prompt constrains the complexity of the hypothesis space, making it easier to find optimal hypotheses and improving suitability for

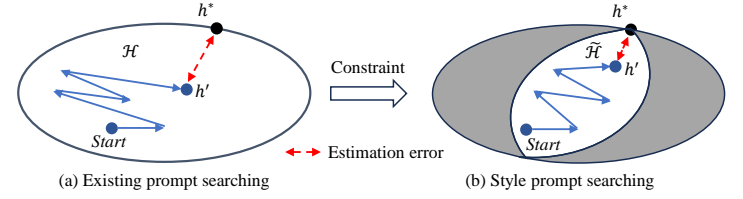


Fig. 3. (a) The standard prompt searching. (b) The style prompt searching. h^* is the expected risk and h' is the empirical risk. \mathcal{H} and $\tilde{\mathcal{H}}$ represent the hypothesis space before and after constraints, respectively. The objective is minimizing the estimation error.

FSL tasks. As shown in Figure 3 (a), existing methods search for optimal prompts in the entire prompt hypothesis space \mathcal{H} . Our goal is to minimize the estimation error. However, this is challenging for the target FSL task. This paper proposes a style prompt to constrain the complexity of \mathcal{H} ($\tilde{\mathcal{H}}$ represents the hypothesis space after constraints) by only adjusting in the style aspect, as shown in Figure 3 (b), which speeds up the searching. Besides, inspired by [50], $\tilde{\mathcal{H}}$ is more conducive to FSL tasks.

3.2.2 Why using Step-wise Distribution Alignment?

Since the source data is inaccessible in SF-CDFSL, explicitly reducing the domain gap between source and target data is impossible. To address the challenges inherent in SF-CDFSL and optimize the prompts, this paper proposes an implicit domain alignment strategy. Specifically, let P_θ denote the initial prediction distribution obtained by the initial pre-trained θ on \mathcal{D}^t . Our aim is to discern the ideal prediction distribution P_t , which is unknown, typically markedly distinct from P_θ (i.e. exhibiting significant distribution gap). Therefore, the problem can be framed as a distribution optimization problem,

$$\arg \min_{\theta} \mathbf{D}(\hat{P}_t, P_t), \quad (1)$$

where \hat{P}_t is the predicted distribution by model, $\mathbf{D}(\cdot, \cdot)$ denotes the discrepancy between two distributions. However, two key challenges arise in this optimization: (1) the unknown nature of P_t complicates optimization efforts, and (2) the substantial domain gap between P_θ and P_t makes achieving satisfactory results through one-step searching for \hat{P}_t difficult [24], [25], [51].

Inspired by [25], [51], this paper converts the challenging one-step search for \hat{P}_t into a multi-step alignment problem.

Specifically, we construct a step-wise prediction distribution flow from P_θ to P_t , denoted as $P_{\theta_0} \rightarrow P_{\theta_1} \rightarrow \dots \rightarrow P_{\theta_e} \rightarrow \dots \rightarrow P_{\theta_E}$, where $P_{\theta_0} = P_\theta$ and $P_{\theta_E} = \hat{P}_t$ with $\theta_E = \theta_t$. Here, θ_e represents the e -th intermediate model estimating P_{θ_e} . Our objective is optimizing Eq. 1, i.e. $\hat{P}_t = P_t$, where \hat{P}_t and P_t share the same label space \mathcal{Y} . Based on Theorem 3.2 in [24]:

Theorem 1. Given distribution P, Q with distance $D(P, Q) = \tau < \frac{1}{R}$ ($\frac{1}{R}$ stands for the regularization strength of models to be learned) and $P(\mathcal{Y}) = Q(\mathcal{Y})$ (no label shift). Suppose P, Q satisfy the bounded data assumption, and we have initial model θ with objective loss $L(\theta, P)$, and n unlabeled samples S from Q , we set $\theta' = ST(\theta, S)$ letting the objective loss $L(\theta', Q) < \alpha^*$ (α^* is a given small loss), then

$$L(\theta', Q) \leq \frac{2}{1 - \tau R} L(\theta, P) + \alpha^* + O\left(\frac{1}{\sqrt{n}}\right). \quad (2)$$

We can know that $L(\theta', Q)$ becomes smaller as τ becomes smaller. However, minimizing τ is difficult when there is large domain gap between P and Q . Hence, this paper, inspired by [25], attempts to convert an optimization problem of τ into that of multiple small $\{\tau_i\}_{i=1}^E$ ($\tau = \sum_{i=1}^E \tau_i$). The performance upper bound is presented in the following Theorem,

Theorem 2. Given a distribution flow from P_{θ_0} to P_{θ_E} , denoted as $P_{\theta_0} \rightarrow P_{\theta_1} \rightarrow \dots \rightarrow P_{\theta_E}$, $P_{\theta_E} = \hat{P}_t$, and $P(\mathcal{Y}) = Q(\mathcal{Y})$, and the data is bounded. Distribution distances are $\{\tau_i\}_{i=1}^E$, and $\tau_m = \max(\{\tau_i\}_{i=1}^E)$, then

$$\begin{aligned} L(\theta_E, P_{\theta_E}) &\leq \frac{2}{1 - \tau_E R} L(\theta_{E-1}, P_{\theta_{E-1}}) + \alpha^* + O\left(\frac{1}{\sqrt{n}}\right), \\ &\leq \frac{2}{1 - \tau_m R} L(\theta_{E-1}, P_{\theta_{E-1}}) + \alpha^* + O\left(\frac{1}{\sqrt{n}}\right), \end{aligned} \quad (3)$$

if source model has low loss $\alpha_0 \geq \alpha^*$ on the source domain, according to the formula for the sum of a geometric series,

$$L(\theta_E, P_{\theta_E}) \leq \left(\frac{2}{1 - \tau_m R}\right)^{E+1} (\alpha_0 + O\left(\frac{1}{\sqrt{n}}\right)). \quad (4)$$

It is worth noting that the tightness of the upper bound in Eq. 4 is closely related to both $\frac{2}{1 - \tau_m R}$ and E , with the factor $\frac{2}{1 - \tau_m R}$ playing a particularly significant role. To better understand the growth characteristics within the recursive process, we apply a Fourier transform to convert the upper bound of Eq. 4 into the frequency domain, allowing for a more intuitive analysis of its stability and convergence, as shown in the following:

$$\begin{aligned} \hat{L}(\omega) &= \sum_{E=0}^{\infty} \left(\frac{2}{1 - \tau_m R}\right)^{E+1} (\alpha_0 + O\left(\frac{1}{\sqrt{n}}\right)) e^{-j\omega E} \\ &= (\alpha_0 + O\left(\frac{1}{\sqrt{n}}\right)) \sum_{E=0}^{\infty} \left(\frac{2}{1 - \tau_m R}\right)^{E+1} e^{-j\omega E} \\ &= (\alpha_0 + O\left(\frac{1}{\sqrt{n}}\right)) \left(\frac{2}{1 - \tau_m R}\right) \sum_{E=0}^{\infty} \left(\frac{2e^{-j\omega}}{1 - \tau_m R}\right)^E \end{aligned} \quad (5)$$

where ω is frequency, and j represents the imaginary part of a complex number. At this point, we convert the exponential function in Eq. 4 into a series summation problem in Eq. 5. To avoid the upper bound divergence, the geometric series in Eq. 5 needs to converge, which requires that $\left|\frac{2e^{-j\omega}}{1 - \tau_m R}\right| < 1$, i.e. $\tau_m R > 3$. The final frequency domain formula for Eq. 5 is,

$$\hat{L}(\omega) = (\alpha_0 + O\left(\frac{1}{\sqrt{n}}\right)) \frac{2}{(1 - \tau_m R) - 2e^{-j\omega}}, \quad (6)$$

with $\tau_m R > 3$.

Eq. 6 shows that, under weak regularization constraints, the upper bound of $L(\theta_E, P_{\theta_E})$ can be decreased by reducing τ_m and ω , where ω is influenced by τ_m because ω reflects the oscillation in the recursive growth, which depends on the size of τ_m . The larger the τ_m , the greater the ω . By introducing condition $\tau_m R > 3$ into Eq. 4, we also can know that $\frac{2}{1 - \tau_m R} < 1$, which means $\left(\frac{2}{1 - \tau_m R}\right)^{E+1} < 1$. Therefore, $L(\theta_E, P_{\theta_E})$ obtains a tight upper bound. However, $\tau_m = \max(\{\tau_i\}_{i=1}^E)$ only can be obtained until the end of flow. Instead of using τ_m , we try to reduce all $\{\tau_i\}_{i=1}^E$ to optimize $L(\theta_E, P_{\theta_E})$. Therefore, a step-wise distribution alignment strategy is proposed to reduce each τ_i , converting the original optimization (Eq. 1) into the multiple following sub-problems:

$$\arg \min_{\theta} \mathbf{D}(P_{\theta_{e-1}}, P_{\theta_e}), \quad e = 1, \dots, E, \quad (7)$$

the e -th sub-problem refers to a single-step search that computes the current prediction distribution P_{θ_e} , given the previous one $P_{\theta_{e-1}}$. In summary, a step-wise distribution alignment strategy is proposed to transform the challenging one-step prediction distribution optimization problem (Eq. 1) into the simple multi-step distribution alignment problem (Eq. 7). This strategy not only simplifies the optimization process but also enhances the model's adaptability to domain shifts. As a result, the proposed strategy offers a more practical and effective solution for improving cross-domain few-shot learning performance.

3.3 StepSPT: Step-wise Distribution Alignment for Style Prompt Tuning

The source model θ maps image samples to a high-dimensional feature space, denoted as $\theta : \mathcal{X}_s \rightarrow \mathbb{R}^{dm}$, where dm is the feature dimension. Additionally, a classifier $\psi : \mathbb{R}^{dm} \rightarrow \mathbb{R}^N$ is then applied, forming $\psi \circ \theta$. This section introduces Step-wise Distribution Alignment guided Style Prompt Tuning (StepSPT), as shown in Figure 2. To minimize learning costs, the parameters of θ remains fixed. Firstly, StepSPT proposes a style prompt ω (Section 3.3.1) to adjust input styles to adapt $\psi \circ \theta$. Besides, StepSPT explores a dual-phase optimization process (Section 3.3.2) including external and internal processes. The external process to optimize ω using a step-wise distribution alignment while keeping $\psi \circ \theta$ frozen. The query set Q is introduced into external process to bridge domain gaps and mitigating overfitting. To avoid error accumulation in the step-wise alignment process, this paper introduces a credible group \mathcal{G} to correct the alignment error between each step. Specifically, some samples in $P_{\theta_{e-1}}$ first are selected through entropy sorting and prototype sorting to form \mathcal{G} , and then the samples in P_{θ_e} are selected by chain-search to be the pairs of samples in \mathcal{G} . Finally, by aligning these data pairs, the interference of noise or erroneous data can be reduced. While the internal process optimizes ψ with only labeled support set S while keeping θ and ω frozen. There can be one external and multiple internal processes in a step. To show the StepSPT process more clearly, Algorithm 1 is shown in Section 3.3.3.

3.3.1 Style Prompt

Given that image style significantly influences domain shift [6], [30], this paper devises a style prompt ω to interact with input images in \mathcal{X} , thereby influencing their style to conform to the desired distribution and adapt to the source model. Unlike existing approaches that treat prompts and input data as independent entities, drawing inspiration from batch normalization's capability to alter image styles, we design the

learnable ω to adjust image styles, as illustrated in the following formulation:

$$x_p = f_p(x) = \omega_1 \frac{x - \mu_{\mathcal{X}}}{\sqrt{\sigma_{\mathcal{X}}^2 + \varepsilon}} + \omega_2, \quad x \in \mathcal{X}, \quad (8)$$

where ω_1 and ω_2 (collectively referred to as ω) are the learnable parameters of style prompt, $\mathcal{X} = \{\mathcal{X}_s, \mathcal{X}_q\}$, $\mu_{\mathcal{X}}$ and $\sigma_{\mathcal{X}}^2$ are the mean and variance of \mathcal{X} ,

$$\mu_{\mathcal{X}} = \frac{1}{m} \sum_{i=1}^m x_i, \quad \sigma_{\mathcal{X}}^2 = \frac{1}{m} \sum_{i=1}^m (x_i - \mu_{\mathcal{X}})^2, \quad (9)$$

where m is the sample number of \mathcal{X} , the obtained x_p is the adjusted x through ω , where ω_1 and ω_2 are updated by a step-wise distribution alignment strategy proposed in the external process, which will be introduced in Section 3.3.2.

3.3.2 Dual-phase Optimization Process

The dual-phase optimization process consists of an external and an internal process. The external process focuses on optimizing ω using the proposed step-wise distribution alignment strategy to implicitly reduce the distance between the source and target domains. Meanwhile, the internal process updates ψ to ensure classification accuracy.

External Process. In the external process, ω is updated while keeping θ and ψ frozen. Since Wasserstein distance is benefit for solving cross-domain problem [52], we employ the Wasserstein distance to quantify distribution shift [24], denoted as $\mathbf{D}_{wass}(\cdot, \cdot)$. For any adjacent distributions, the shift measure for N -way classification is expressed as:

$$\begin{aligned} \mathbf{D}_{wass}(P_{\omega_{e-1}}, P_{\omega_e}) &= \max \{d_0, \dots, d_n, \dots, d_{N-1}\}, \\ d_n &= \mathbf{W}_{\infty}(P_{\omega_{e-1}}(x^{e-1} | y^{e-1} = n), P_{\omega_e}(x^e | y^e = n)), \end{aligned} \quad (10)$$

where $\mathbf{W}_{\infty}(\cdot, \cdot)$ denotes the Wasserstein-infinity distance, x^{e-1} and x^e represent samples satisfying $P_{\omega_{e-1}}$ and P_{ω_e} respectively, while y^{e-1} and y^e denote labels. The conditional distributions $P_{\omega_{e-1}}(x^{e-1} | y^{e-1} = n)$ and $P_{\omega_e}(x^e | y^e = n)$ represent the probability metrics for the n -th category according to $P_{\omega_{e-1}}$ and P_{ω_e} , respectively. For each of the N categories, we calculate the Wasserstein-infinity distances and identify the largest distance to quantify the distribution shift. However, in the query set Q , precise category labels are unavailable. To overcome this challenge, we aim to minimize the distances $\{d_0, \dots, d_n, \dots, d_{N-1}\}$ without depending on category labels, as described by the following equation:

$$\begin{aligned} d_e &= \mathbf{W}_{\infty}(P_{\omega_{e-1}}(x^{e-1} | y^{e-1}), P_{\omega_e}(x^e | y^e)), \\ \text{with} \quad y^{e-1} &= y^e, \end{aligned} \quad (11)$$

Since $P_{\omega_{e-1}}$ is not aligned with P_t , which means not all samples in $P_{\omega_{e-1}}$ are credible. Therefore, addressing the minimization of d_e involves two key challenges: (1) determining the credible data pairs supporting d_e estimation, and (2) reducing d_e using these data pairs.

The proposed step-wise distribution alignment strategy addresses these challenges with two components: (1) Distribution gap estimation and (2) Distribution alignment.

(1) *Distribution Gap Estimation.* In the distribution gap estimation phase, as the distribution in $P_{\theta_{e-1}}$ may not align with the optimal target distribution, the initial task in distribution gap estimation is to establish a credible group \mathcal{G} within $P_{\theta_{e-1}}$ as a trusted distribution label, as shown in "Credible group generation in $P_{\theta_{e-1}}$ " part of Figure 4 (a). This entails ensuring that samples exhibit high confidence in specific categories through self-supervised or unsupervised methods. Data from

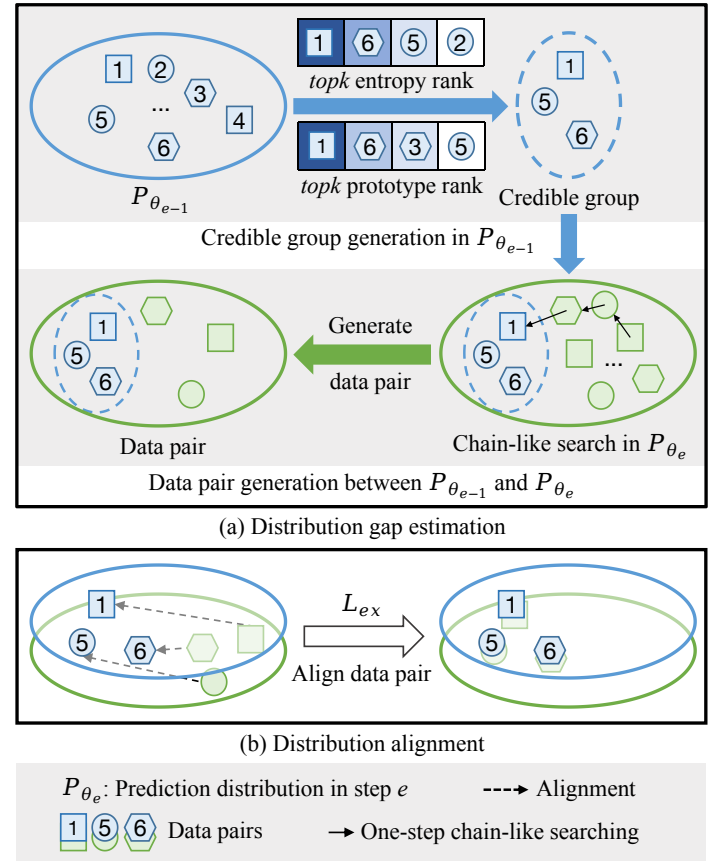


Fig. 4. Overview of Step-wise distribution alignment strategy. The goal is align the examples from P_{θ_e} to that from $P_{\theta_{e-1}}$. We achieve it through two stages: (a) Distribution gap estimation, and (b) Distribution alignment. The color gradient from dark to light represents the ranking from the best choice to the worst choice.

P_{θ_e} is then matched to \mathcal{G} to form credible data pairs. Two methods are used to create \mathcal{G} : entropy-based ranking [53], [54] and prototype-based ranking [55].

Initially, we generate the entropy-based ranking credible group \mathcal{G}_{en} as follows:

$$\mathcal{G}_{en} = \{\mathbf{p}_i | \mathbf{p}_i \in P_{\theta_{e-1}}, i \in \text{topk}(H, \alpha \cdot m)\}, \quad (12)$$

where $H = \{h_i\}_{i=1}^m$ is an entropy set, with $h_i = -\sum \mathbf{p}_i \log \mathbf{p}_i$, $\mathbf{p}_i = \psi \circ \theta \circ \omega(x_i)$ and $x_i \in \mathcal{X}$, while m denotes the number of samples, and $\text{topk}(H, \alpha \cdot m)$ selects the top $\alpha \cdot m$ lowest elements from H .

However, as shown in Figure 5, the entropy-based group \mathcal{G}_{en} has a many-to-one problem of prediction distributions and entropy values, making \mathcal{G}_{en} redundant and ambiguous. For example, in the Figure 5, we should choose the top 4 entropy samples. However, there are the same entropy value for the samples 6, 5, 2, 3, and they are tied for second place, i.e. there is currently one entropy value (0.21) corresponding to multiple samples (6, 5, 2, 3). One of them needs to be excluded, and there is no indicator that can determine which sample is excluded. We alleviate this problem from the class-aware dimension. Specifically, a prototype-based ranking credible group \mathcal{G}_{pro} is introduced as follows,

$$\mathcal{G}_{pro} = \{\mathbf{p}_i | \mathbf{p}_i \in P_{\theta_{e-1}}, i \in \text{topk}(A, \gamma \cdot m)\}, \quad (13)$$

where $\text{topk}(A, \gamma \cdot m)$ means select the top $\gamma \cdot m$ samples from $A = \{a_i\}_{i=1}^m$ over the target data, $a_i = \min(\mathbf{v}_i)$, where $\mathbf{v}_i =$

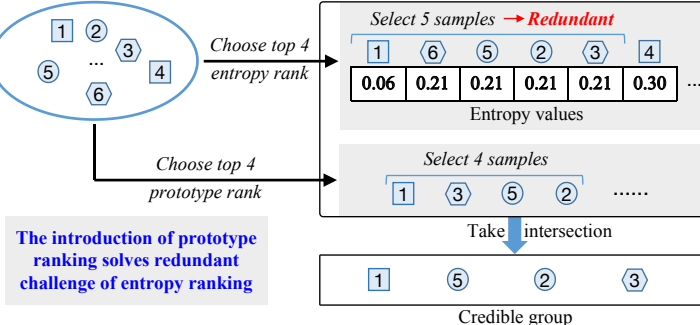


Fig. 5. Problem of only using \mathcal{G}_{en} . Samples 6, 5, 2, 3 have the same entropy values, the top 4 selection of \mathcal{G}_{en} become redundant and ambiguous. The introduction of prototype ranking \mathcal{G}_{pro} can address this challenge.

$\{v_{i,1}, v_{i,2}, \dots, v_{i,N}\}$, with $v_{i,n}$ is the cosine distance between the feature vector \mathbf{p}_i and the prototype \mathbf{o}_n , calculated as follows:

$$v_{i,n} = \cos(\mathbf{p}_i, \mathbf{o}_n) = \frac{\mathbf{p}_i \cdot \mathbf{o}_n}{\|\mathbf{p}_i\| \|\mathbf{o}_n\|}, \quad (14)$$

and \mathbf{o}_n is obtained by,

$$\mathbf{o}_n = \frac{1}{K} \sum_{k=1}^K \psi \circ \theta \circ \omega(S), \quad (15)$$

Finally, the credible group \mathcal{G} is obtained by an intersection operation as $\mathcal{G} = \mathcal{G}_{pro} \cap \mathcal{G}_{en}$.

We then match the examples in P_{θ_e} to \mathcal{G} . To construct the data pairs between P_{θ}^e and P_{θ}^{e-1} , the credible neighbor \mathbf{p}'_i from \mathcal{G} is identified through a chain-like search for \mathbf{p}_i (from P_{θ_e}). Specifically, beginning with \mathbf{p}_i , we perform a one-step search to find its nearest neighbor $\hat{\mathbf{p}}_i^1$, based on cosine distance. If $\hat{\mathbf{p}}_i^1$ does not belong to \mathcal{G} , we conduct another search for a new nearest neighbor $\hat{\mathbf{p}}_i^2$ starting with $\hat{\mathbf{p}}_i^1$. This process continues iteratively until we reach \mathcal{G} , resulting in a search flow $\mathbf{p}_i \rightarrow \hat{\mathbf{p}}_i^1 \rightarrow \hat{\mathbf{p}}_i^2 \rightarrow \dots \rightarrow \mathbf{p}'_i$. Here, $\mathbf{p}'_i \in \mathcal{G}$ serves as the data pair of \mathbf{p}_i , as shown in "Data pair generation between $P_{\theta_{e-1}}$ and P_{θ_e} " part of Figure 4 (a).

(2) *Distribution Alignment*. During distribution alignment, we mitigate distribution shift by aligning these data pairs under the category consistency constraint. Inspired by the theoretical link between mutual information and pairwise losses [56], we use the following objective to achieve our goal,

$$L_{MI}(\omega_e) = \min_{\omega_e} [-I(\mathbf{p}_i, \mathbf{p}'_i)], \quad (16)$$

Here, $I(\cdot, \cdot)$ denotes the mutual information function [57], computed similarly to [58]. Given that limited data may not adequately represent the probability distribution, optimizing solely based on L_{MI} is restricted. To address this, we introduce a diversity loss to promote balanced category predictions [59],

$$L_{KL}(\omega_e) = \min_{\omega_e} \sum_{n=1}^N KL(\bar{\mathbf{p}}_n, \frac{1}{N}). \quad (17)$$

Here, $KL(\cdot, \cdot)$ denotes the KL-divergence loss function, and $\bar{\mathbf{p}}_n = \frac{1}{m} \sum_{i=1}^m \mathbf{p}_{i,n}$ represents the empirical label distribution, where $\mathbf{p}_{i,n}$ is the probability of x_i in the n -th category. The final objective in the external process is:

$$L_{ex}(\omega_e) = L_{MI}(\omega_e) + \sigma L_{KL}(\omega_e), \quad (18)$$

where σ is a weight value of L_{KL} . The distribution alignment is summarized in the Figure 4 (b). Generally, the external process adjusts the style prompt ω through step-wise distribution alignment, allowing the model to progressively adapt to domain

Algorithm 1 StepSPT process.

Input: Support set $(\mathcal{X}_s, \mathcal{Y}_s)$, query set \mathcal{X}_q , initialized style prompt ω_0 , frozen encoder θ , and initialized classifier ψ_0 .

Output: Optimized style prompt ω and classifier ψ .

$\mathbf{p}_i = \psi_0 \circ \theta \circ \omega_0(x_i), \quad x_i \in \{\mathcal{X}_s, \mathcal{X}_q\}, \mathbf{p}_i \in P_{\omega_0}$

For $step=1, \dots, e, \dots, E$ **do**

- Calculate the entropy h_i and prototype centers \mathbf{o}_n in $P_{\omega_{e-1}}$
- Get a_i and \mathbf{o}_n in $P_{\omega_{e-1}}$
- Get $H = \{h_i\}_{i=1}^m$ and $A = \{a_i\}_{i=1}^m$
- Get $\mathcal{G}_{en} = \{\mathbf{p}_i | \mathbf{p}_i \in P_{\omega_{e-1}}, i \in \text{topk}(H, \alpha \cdot m)\}$
- Get $\mathcal{G}_{pro} = \{\mathbf{p}_i | \mathbf{p}_i \in P_{\omega_{e-1}}, i \in \text{topk}(A, \gamma \cdot m)\}$
- Get the final credible group $\mathcal{G} = \mathcal{G}_{pro} \cap \mathcal{G}_{en}$

for $epoch=1, \dots, \text{max epochs}/E$ **do**

- for** each mini-batch $\{x_i, y_i\}$ in $(\mathcal{X}_s, \mathcal{Y}_s)$ **do**
- $\mathbf{p}_i = \psi_{e-1} \circ \theta \circ \omega_{e-1}(x_i)$,
- Compute Eq. 19 and update ψ_{e-1} as ψ_e ;
- end for**

end for

$\mathbf{p}_i = \psi_e \circ \theta \circ \omega_{e-1}(x_i), \quad x_i \in \{\mathcal{X}_s, \mathcal{X}_q\}$

Search data pairs \mathbf{p}'_i in \mathcal{G} for \mathbf{p}_i through a chain-like search

Compute Eq. 18 with $(\mathbf{p}_i, \mathbf{p}'_i)$ and update ω_{e-1} as ω_e

$\omega_{e-1} = \omega_e, \psi_{e-1} = \psi_e, P_{\omega_{e-1}} = P_{\omega_e}$

end for

shifts and maintain robust performance across different data distributions.

Internal Process. Following the style prompt updates, the classifier ψ is optimized using cross-entropy loss solely with S in the internal process, keeping $\theta \circ \omega$ frozen. The cross-entropy loss is as follows:

$$L_{in}(\psi_e) = CE(\psi_e \circ \theta | \omega_{e-1}(x_i)) = - \sum_{i=1}^{N \times K} y_i \log \mathbf{p}_i. \quad (19)$$

where $\mathbf{p}_i = \theta \circ \omega_{e-1}(x_i)$, $\{x_i, y_i\} \subset S$, and $N \times K$ means the number of support set S . There can be multiple internal processes in a step, which shows the iterative nature of the optimization and emphasizes the importance of refining the classifier ψ to achieve stable and accurate predictions.

3.3.3 Overall Pipeline of StepSPT

Algorithm 1 presents the overall pipeline of StepSPT, highlighting both the internal and external processes. Initially, the support set $(\mathcal{X}_s, \mathcal{Y}_s)$ and query set \mathcal{X}_q are provided as input, along with the style prompt ω_0 and classifier ψ_0 , which are randomly initialized. The encoder ω remains frozen and is sourced from a pre-trained model using source data to ensure stable feature extraction. The initial prediction $\mathbf{p}_i = \psi_0 \circ \theta \circ \omega_0(x_i)$ is calculated for each $x_i \in \{\mathcal{X}_s, \mathcal{X}_q\}$. This step helps identify credible samples based on entropy h_i and prototype centers \mathbf{o}_n , forming the credible group \mathcal{G} . The internal process (highlighted in blue in Algorithm 1) iteratively optimizes the classifier ψ using cross-entropy loss for a specified number of epochs, $\text{max epochs}/E$. This step is essential for refining the model's performance on the support set. After the internal process, the external process utilizes the updated classifier ψ and credible group \mathcal{G} to optimize the style prompt ω through the step-wise distribution alignment strategy. This strategy helps the model better align with the target domain, ensuring that the learned representations maintain robustness across different data distributions. By alternating between the internal and external processes, StepSPT progressively improves the style prompt and classifier, ultimately achieving better CDFSL performance.

TABLE 1

Comparison between prompt-tuning based methods and StepSPT in 5-way 1-shot and 5-way 5-shot tasks. **Backbone** indicates the utilized backbone in the method. Cells highlighted in blue indicate the best performance achieved with each respective backbone.

Task	Methods	Backbone	CropDisease	EuroSAT	ISIC	ChestX	PatternNet	Avg
5-way 1-shot	Finetuning [26]	ResNet10	65.70 \pm 0.85	63.44 \pm 0.83	33.67 \pm 0.60	22.70 \pm 0.41	76.06 \pm 0.89	52.38
	IM-DCL [17]	ResNet10	74.23 \pm 0.91	69.91 \pm 0.92	34.23 \pm 0.65	22.89 \pm 0.43	76.68 \pm 0.87	55.58
	StepSPT (Ours)	ResNet10	78.35 \pm 0.53	68.21 \pm 0.42	35.11 \pm 0.63	22.83 \pm 1.03	77.83 \pm 0.95	56.47
	ViT [12]	ViT	78.39 \pm 0.88	58.60 \pm 0.78	30.74 \pm 0.54	21.90 \pm 0.91	68.13 \pm 0.91	51.55
	VPT [40]	ViT	75.00 \pm 0.24	67.53 \pm 0.59	30.80 \pm 0.96	20.56 \pm 0.64	79.87 \pm 0.69	54.75
	StepSPT (Ours)	ViT	82.56 \pm 0.27	68.47 \pm 0.22	32.03 \pm 0.42	23.55 \pm 1.06	80.84 \pm 0.31	57.49
	CLIP [11]	CLIP	78.93 \pm 0.83	66.88 \pm 0.80	30.45 \pm 0.55	21.63 \pm 0.39	91.71 \pm 0.55	57.92
	CoOp [41]	CLIP	75.25 \pm 1.60	70.00 \pm 1.15	30.45 \pm 0.59	20.91 \pm 0.31	90.24 \pm 0.57	57.37
	CoCoOp [42]	CLIP	75.37 \pm 0.78	71.56 \pm 0.85	30.07 \pm 0.36	20.23 \pm 0.84	90.55 \pm 0.31	57.56
	StepSPT (Ours)	CLIP	84.84 \pm 0.72	70.01 \pm 0.21	32.97 \pm 0.27	22.84 \pm 0.95	95.16 \pm 0.51	61.16
5-way 5-shot	ConvNeXt [61]	ConvNeXt	91.35 \pm 0.64	66.25 \pm 0.77	33.13 \pm 0.53	22.11 \pm 0.55	91.93 \pm 0.25	60.95
	StepSPT (Ours)	ConvNeXt	95.39 \pm 0.22	73.83 \pm 0.80	37.16 \pm 0.68	23.73 \pm 0.98	96.44 \pm 0.42	65.31
	Finetuning [26]	ResNet10	88.16 \pm 0.55	81.65 \pm 0.63	45.87 \pm 0.64	25.77 \pm 0.43	92.86 \pm 0.39	66.86
	IM-DCL [17]	ResNet10	88.68 \pm 0.58	82.90 \pm 0.85	45.58 \pm 0.83	25.98 \pm 0.47	93.03 \pm 0.58	67.23
	StepSPT (Ours)	ResNet10	88.84 \pm 0.41	82.91 \pm 0.32	46.41 \pm 0.75	27.56 \pm 0.90	93.35 \pm 1.03	67.81
	ViT [12]	ViT	95.27 \pm 0.37	77.99 \pm 0.57	47.66 \pm 0.59	25.74 \pm 0.41	92.77 \pm 0.36	67.89
	VPT [40]	ViT	95.20 \pm 0.99	78.05 \pm 0.39	50.00 \pm 0.44	26.63 \pm 1.03	93.24 \pm 0.74	68.62
	StepSPT (Ours)	ViT	97.07 \pm 0.75	84.88 \pm 0.28	50.39 \pm 0.34	26.65 \pm 0.11	95.96 \pm 0.65	70.99
	CLIP [11]	CLIP	92.53 \pm 0.35	86.49 \pm 0.82	48.67 \pm 0.44	25.16 \pm 0.35	98.58 \pm 0.59	70.29
	CoOp [41]	CLIP	89.26 \pm 1.60	85.97 \pm 0.95	46.40 \pm 0.85	25.37 \pm 0.94	98.08 \pm 0.58	69.02
	CoCoOp [42]	CLIP	90.20 \pm 0.34	86.07 \pm 0.62	46.99 \pm 0.71	26.15 \pm 0.83	98.71 \pm 0.40	69.62
	StepSPT (Ours)	CLIP	96.01 \pm 0.88	89.40 \pm 1.05	52.12 \pm 0.36	26.36 \pm 0.97	99.04 \pm 0.31	72.58
	ConvNeXt [61]	ConvNeXt	95.15 \pm 0.29	88.11 \pm 0.90	52.51 \pm 0.48	26.57 \pm 0.21	98.52 \pm 0.36	72.17
	StepSPT (Ours)	ConvNeXt	97.11 \pm 0.60	91.07 \pm 0.73	53.99 \pm 0.44	27.11 \pm 0.75	99.24 \pm 0.32	73.79

4 EXPERIMENTS

In this section, we introduce the datasets and implementation details. We then present the results of StepSPT, including comparisons with prompt-based methods and SOTAs, the ablation study, and the extra performance analysis.

4.1 Implementation

4.1.1 Datasets

StepSPT is evaluated across 4 datasets from the BSCD-FSL benchmark [26] and an additional dataset, PatternNet [60]. Within the BSCD-FSL scope, domain similarity to scene imagery progressively diminishes from CropDisease to ChestX, spanning a range from natural environments to medical images. Furthermore, the lower resolution of EuroSAT samples highlights a potential concern: its performance could be enhanced by increasing image resolution, rather than addressing the cross-domain challenge. To demonstrate that the proposed method genuinely solves the cross-domain problem, this paper includes the high-resolution PatternNet dataset in the evaluation, showcasing the superior performance of the proposed StepSPT on high-resolution remote sensing data. PatternNet is a large-scale high-resolution remote sensing dataset collected for remote sensing image retrieval. There are 38 classes and each class has 800 images of size 256×256 pixels.

4.1.2 Implementation Details

We average the StepSPT evaluation results for 600 episodes, where each episode contains 100 epochs. We show the performance with average accuracy and 95% confidence interval. Besides, We used NVIDIA A100 GPUs, each with 40GB of memory. Each experiment was run on a single GPU. On average, each training run of 600 episodes (with ConvNeXt backbone) took approximately 6 hours for 1-shot tasks and 16 hours for 5-shot tasks, respectively. A linear classifier is utilized for classification. We utilize Stochastic Gradient Descent (SGD) with a learning rate of 0.01, momentum of 0.9, and weight decay of 10^{-3} for updating the prompt and classifier. α and γ are set to 0.7 and 0.4, respectively, with σ set to 2. To enhance outcomes further, we incorporate label propagation (LP) into our method. Furthermore, StepSPT is evaluated on both 5-way 1-shot and 5-way 5-shot tasks.

4.2 Compare with prompt tuning-based methods

Our evaluation of StepSPT begins by comparing with the baseline and existing prompt tuning-based methods. To ensure objective assessments, we first present the baselines on the backbones of ResNet10, ViT [12], CLIP [11], and ConvNeXt [61]. All baselines keep the backbone parameters fixed. We use only the image encoder in CLIP, followed by a linear classifier, to evaluate its CDFSL performance. Then we compare StepSPT with the prompt based methods such as VPT [40], CoOp [41], CoCoOp [42]. Finally, we present the performance of StepSPT on different pretrained backbones, including ViT-base-16¹, CLIP with ViT-32², and ConvNeXt-Xlarge³. The outcomes for both 5-way 1-shot and 5-way 5-shot tasks are detailed in Table 1.

As shown in Table 1, in the 5-way 1-shot task, the average performance across the four baselines, ranked from highest to lowest, is as follows: ConvNeXt \geq CLIP \geq ResNet10 \geq ViT. In comparison to near-domain tasks like CropDisease, EuroSAT, and PatternNet, both ResNet10 and ConvNeXt perform better than ViT and CLIP in the distant domain like ISIC and ChestX. For example, the ResNet10 and ConvNeXt baselines achieve 33.67% and 33.13% on ISIC, outperforming ViT and CLIP, which achieve 30.74% and 30.45%, respectively, on ISIC. Furthermore, the performance of ResNet10 and ConvNeXt baselines on ChestX (22.70% and 22.11%) are higher than those of ViT and CLIP baselines on ChestX (21.90% and 21.63%). It shows that compared to Transformer-based backbones (ViT and CLIP), CNN-based backbones (ResNet10 and ConvNeXt) demonstrate greater advantages in handling cross-domain tasks. This trend is also observable in the current prompt tuning-based methods, including StepSPT. This difference may stem from the tendency of Transformer architectures to focus on extracting global information. In contrast, CNNs [61], [62] excel at simultaneously capturing both local and global features. While the strong transferability of local features makes them particularly critical for cross-domain tasks, which contributes to the superior performance of CNN-based backbones in these scenarios. Additionally, we observe that for near-domain tasks such as CropDisease, EuroSAT, and PatternNet, while methods

1. https://github.com/google-research/vision_transformer

2. <https://github.com/openai/CLIP>

3. <https://github.com/huggingface/pytorch-image-models/tree/main/timm>

TABLE 2

Comparison between SOTA methods and StepSPT in the 5-way 1-shot and 5-way 5-shot tasks. **SF** means if the method is source-free. **Backbone** indicates the utilized backbone in the method. **Freeze** exhibits if the backbone is frozen. 'Y' means yes, '-' means no.

Task	Methods	SF	Backbone	Freeze	CropDisease	EuroSAT	ISIC	ChestX	PatternNet	Avg
5-way 1-shot	Finetuning [26]	-	ResNet10	-	68.46 \pm 0.87	59.18 \pm 0.85	33.11 \pm 0.60	22.54 \pm 0.42	79.23 \pm 0.79	52.51
	LRP [27]	-	ResNet10	-	59.23 \pm 0.50	54.99 \pm 0.50	30.94 \pm 0.30	22.11 \pm 0.20	-	-
	FDMixup [28]	-	ResNet10	-	66.23 \pm 1.03	62.97 \pm 1.01	32.48 \pm 0.64	22.26 \pm 0.45	-	-
	FWT [2]	-	ResNet10	-	66.36 \pm 1.04	62.36 \pm 1.05	31.58 \pm 0.67	22.04 \pm 0.44	-	-
	STARTUP [3]	-	ResNet10	-	75.93 \pm 0.80	63.88 \pm 0.84	32.66 \pm 0.60	23.09 \pm 0.43	-	-
	LDP-Net [63]	-	ResNet10	-	69.64	65.11	33.97	23.01	-	-
	DDA [4]	-	ResNet10	-	82.14 \pm 0.78	73.14 \pm 0.84	34.66 \pm 0.58	23.38 \pm 0.43	-	-
	StyleAdv [6]	-	ResNet10	-	80.69 \pm 0.28	72.92 \pm 0.75	35.76 \pm 0.52	22.64 \pm 0.35	-	-
	KT [64]	-	ResNet10	-	73.10 \pm 0.87	66.43 \pm 0.93	34.06 \pm 0.77	22.68 \pm 0.60	-	-
	ReFine [65]	-	ResNet10	-	68.93 \pm 0.84	64.14 \pm 0.82	35.30 \pm 0.59	22.48 \pm 0.41	-	-
	VDB [23]	-	ResNet10	Y	71.98 \pm 0.82	63.60 \pm 0.87	35.32 \pm 0.65	22.99 \pm 0.44	-	-
	RDC [8]	-	ResNet10	-	86.33 \pm 0.50	71.57 \pm 0.50	35.84 \pm 0.40	22.27 \pm 0.20	-	-
	CLDFD [66]	-	ResNet10	-	90.48 \pm 0.72	82.52\pm0.76	39.70\pm0.69	22.39 \pm 0.44	94.94 \pm 0.61	66.01
	DARA [9]	-	ResNet10	-	80.74 \pm 0.76	67.42 \pm 0.80	36.42 \pm 0.64	22.92 \pm 0.40	94.44 \pm 0.72	60.39
	IM-DCL [17]	Y	ResNet10	-	84.37 \pm 0.99	77.14\pm0.71	38.13\pm0.57	23.98\pm0.79	96.32\pm0.63	63.99
	DARA [9]	-	ConvNeXt	Y	91.80 \pm 0.85	69.54 \pm 0.62	34.99 \pm 0.53	22.66 \pm 0.75	93.49 \pm 0.65	62.50
	IM-DCL [17]	Y	ConvNeXt	Y	95.13\pm0.95	71.27 \pm 0.42	36.53 \pm 0.93	23.53 \pm 0.26	93.47 \pm 0.57	63.99
	StepSPT (Ours)	Y	ConvNeXt	Y	95.39\pm0.22	73.83 \pm 0.80	37.16 \pm 0.68	23.73 \pm 0.98	96.44\pm0.42	65.31
5-way 5-shot	Finetuning [26]	-	ResNet10	-	89.25 \pm 0.51	79.08 \pm 0.61	48.11 \pm 0.64	25.97 \pm 0.41	95.32 \pm 0.32	67.55
	LRP [27]	-	ResNet10	-	86.15 \pm 0.40	77.14 \pm 0.40	44.14 \pm 0.40	24.53 \pm 0.30	-	-
	FDMixup [28]	-	ResNet10	-	87.27 \pm 0.69	80.48 \pm 0.79	44.28 \pm 0.66	24.52 \pm 0.44	-	-
	FWT [2]	-	ResNet10	-	87.11 \pm 0.67	83.01 \pm 0.79	43.17 \pm 0.70	25.18 \pm 0.45	-	-
	Confess [67]	-	ResNet10	-	88.88 \pm 0.51	84.65 \pm 0.38	48.85 \pm 0.29	27.09 \pm 0.24	-	-
	STARTUP [3]	-	ResNet10	-	93.02 \pm 0.45	82.29 \pm 0.60	47.22 \pm 0.61	26.94 \pm 0.44	-	-
	LDP-Net [63]	-	ResNet10	-	91.89	84.05	48.44	26.88	-	-
	DDA [4]	-	ResNet10	-	95.54 \pm 0.38	89.07 \pm 0.47	49.36 \pm 0.59	28.31\pm0.46	-	-
	StyleAdv [6]	-	ResNet10	-	96.51 \pm 0.28	91.64\pm0.43	53.05 \pm 0.54	26.24 \pm 0.35	-	-
	KT [64]	-	ResNet10	-	89.53 \pm 0.58	82.53 \pm 0.66	46.37 \pm 0.77	26.79 \pm 0.61	-	-
	ReFine [65]	-	ResNet10	-	90.75 \pm 0.49	82.36 \pm 0.57	51.68 \pm 0.63	26.76 \pm 0.42	-	-
	VDB [23]	-	ResNet10	Y	90.77 \pm 0.49	82.06 \pm 0.63	48.72 \pm 0.65	26.62 \pm 0.45	-	-
	RDC [8]	-	ResNet10	-	93.55 \pm 0.30	84.67 \pm 0.30	49.06 \pm 0.30	25.48 \pm 0.20	-	-
	CLDFD [66]	-	ResNet10	-	96.58\pm0.39	92.39\pm0.34	52.29 \pm 0.62	25.98 \pm 0.43	99.00 \pm 0.28	73.35
	DARA [9]	-	ResNet10	-	95.32 \pm 0.34	85.84 \pm 0.54	56.28\pm0.66	27.54 \pm 0.42	99.26\pm0.22	72.85
	IM-DCL [17]	Y	ResNet10	-	95.73\pm0.38	89.47\pm0.42	52.74 \pm 0.69	28.93\pm0.41	99.00 \pm 0.85	73.17
	DARA [9]	-	ConvNeXt	Y	95.65 \pm 0.25	82.12 \pm 0.26	50.80 \pm 0.86	26.37 \pm 0.51	98.62 \pm 0.37	70.71
	IM-DCL [17]	Y	ConvNeXt	Y	97.33\pm0.33	84.53 \pm 0.90	54.33 \pm 0.37	26.40 \pm 0.98	99.00 \pm 0.42	72.32
	StepSPT (Ours)	Y	ConvNeXt	Y	97.11 \pm 0.60	91.07 \pm 0.73	53.99 \pm 0.44	27.11\pm0.75	99.24 \pm 0.32	73.79

based on ViT (78.39% for CropDisease) and CLIP (78.93% for CropDisease) outperform those using ResNet10 (765.70% for CropDisease), they still fall short compared to approaches leveraging ConvNeXt (91.35% for CropDisease). This can be attributed to the ability of ConvNeXt to combine the strengths of CNNs for local feature extraction and Transformers for global feature extraction, capturing both fine-grained details and broad contextual information, essential for generalizing across domains. Importantly, introducing prompts improves baseline results. For instance, VPT is 3.2% higher than ViT on average. The style prompt in StepSPT further demonstrates the powerful impact of adaptive prompts on cross-domain downstream tasks.

Similar to the 5-way 1-shot task, the average performance ranking of the baselines of different backbones on the 5-shot task is: ConvNeXt (72.17%) \geq CLIP (70.29%) \geq ViT (67.89%) \geq ResNet10 (66.86%). However, in the 5-way 5-shot task, CNN models no longer consistently outperform on distant domains. For instance, ViT (47.66%) and CLIP (48.67%) perform better than ResNet10 (45.87%) on ISIC. This outcome can be attributed to the advantages of Transformer models when larger data volumes are available. As a result, in 5-way 5-shot tasks, where the volume of data increases, the strengths of Transformer-based models become more evident. Furthermore, the prompt-based algorithms, with the exception of CoOp and CoCoOp, show performance improvements over their corresponding backbone baselines. Moreover, the proposed StepSPT outperforms all baseline and existing prompt-based methods on all datasets. StepSPT with the ConvNeXt backbone achieves the highest average performance (73.79%) in the 5-way 5-shot task, indicating that ConvNeXt offers significant

advantages for CDFSL tasks over other backbones like ResNet10 and ViT. Therefore, the combined capabilities of ConvNeXt make it the optimal choice for CDFSL tasks in this paper.

4.3 Compare with State-of-the-art

This section primarily compares StepSPT with existing state-of-the-art (SOTA) methods, as shown in Table 2. However, ensuring fairness in these comparisons presents certain challenges. Specifically, most existing SOTA methods are validated on ResNet10, require access to source domain data, and employ specific training strategies to enhance cross-domain transferability. Additionally, these methods fine-tune the model during the adaptation stage. In contrast, the method proposed in this paper follows a source-free setting, which does not require access to source domain data or the use of specific training strategies. Additionally, it keeps the backbone parameters fixed during adaptation, without any fine-tuning. Based on the experimental results in Section 4.2, we chose ConvNeXt as the backbone instead of ResNet10. These setting differences make direct comparisons between StepSPT and existing SOTA methods challenging under varying conditions.

In this scenario, enforcing uniform comparison conditions might obscure each method's performance in its preferred setup. To ensure fairness, we present each method's optimal results to better evaluate their performance under ideal conditions. To further enhance transparency, we also include results for two SOTA approaches (IM-DCL and DARA) on ConvNeXt, providing a balanced view of performance across backbones.

As shown in Table 2, in the 5-way 1-shot task, the proposed StepSPT achieves a sub-optimal average result (65.31%)

TABLE 3

Performance of style prompt and step-wise distribution alignment strategy.

K	Strategy	CropDisease	EuroSAT	ISIC	ChestX	PatternNet	Average
1	Baseline	91.35 \pm 0.64	66.25 \pm 0.77	33.13 \pm 0.53	22.11 \pm 0.55	91.93 \pm 0.25	60.95
	w/o Step	94.95 \pm 0.32	73.24 \pm 0.85	35.37 \pm 0.25	22.75 \pm 0.19	94.59 \pm 0.41	64.11
	w/o Style	93.38 \pm 0.50	73.11 \pm 0.34	36.67 \pm 0.86	22.76 \pm 0.12	93.96 \pm 0.81	63.98
5	StepSPT	95.39 \pm 0.22	73.83 \pm 0.80	37.16 \pm 0.68	23.73 \pm 0.98	96.44 \pm 0.42	65.31
	Baseline	95.15 \pm 0.29	88.11 \pm 0.90	52.51 \pm 0.48	26.57 \pm 0.21	98.52 \pm 0.36	72.17
	w/o Step	98.49 \pm 0.56	90.47 \pm 0.43	52.88 \pm 0.53	26.61 \pm 0.81	99.12 \pm 0.83	73.50
	w/o Style	96.71 \pm 0.85	90.47 \pm 0.57	52.24 \pm 0.83	26.27 \pm 0.93	98.82 \pm 0.34	73.10
	StepSPT	97.11 \pm 0.60	91.07 \pm 0.73	53.99 \pm 0.44	27.11 \pm 0.75	99.24 \pm 0.32	73.70

compared to current SOTAs. Notably, StepSPT performs best on near-domain tasks, achieving optimal results of 95.39% and 96.44% on CropDisease and PatternNet, respectively. However, StepSPT achieves the third-best performance on EuroSAT (73.83%) and ISIC (37.16%). Specifically, a comparison of StepSPT’s results on EuroSAT and PatternNet reveals that the lower sample resolution in EuroSAT leads to a third-best result, whereas high-resolution samples in PatternNet yield the best performance. Additionally, unlike other datasets with clean backgrounds, ISIC images are susceptible to background interference. For instance, in the ‘melanocytic nevus’ category, images containing hair may cause the model to misidentify hair as a pathological feature. This means the model’s attention on ISIC images can be easily distracted by background elements, such as hair, leading to performance degradation. We will discuss this in Section 4.5.3. Moreover, compared to ConvNeXt-based DARA and IM-DCL, StepSPT achieves the best performance.

Furthermore, in the 5-way 5-shot task, StepSPT achieves the highest average performance at 73.79%. StepSPT maintains strong, though not the best, performance on near-domain tasks, with sub-optimal results of 97.11% for CropDisease and 99.24% for PatternNet, indicating that StepSPT’s advantage in the near domain diminishes as data volume increases. Similar to the 5-way 1-shot task, StepSPT also obtains the third-best results on distant domain due to the sample characteristics discussed above. Additionally, StepSPT (73.79%) outperforms ConvNeXt-based DARA (70.71%) and IM-DCL (72.32%) on average.

4.4 Ablation Study

4.4.1 Performance of Style Prompt

We evaluate the performance of the style prompt from three perspectives. First, we demonstrate the advantages of the style prompt by comparing results with and without it. Next, we compare the proposed style prompt with other prompts, including CoOp and CoCoOp. Finally, we visualize the statistical differences in samples with and without the style prompt.

w/ and w/o Style Prompt. We indicate the results of *w/* or *w/o* prompt in Table 3. Compared to the Baseline’ (60.95% and 72.17% average results on 5-way 1-shot and 5-way 5-shot tasks), the style prompt (*w/o Step*) improves performance on all datasets and overall (64.11% and 73.50% on average), demonstrating the effectiveness of prompts for the CDFSL task. The impact of the style prompt can also be evaluated by comparing *w/o Style*’ and StepSPT,’ where StepSPT’ consistently outperforms *w/o Style*’ across all datasets (e.g., 0.4% higher on CropDisease, 0.6% on EuroSAT, 1.75% on ISIC, 0.84% on ChestX, 0.42% on PatternNet, and 0.6% higher on average in the 5-way 5-shot task). This comparison clearly demonstrates the positive role of the style prompt combined with the step-wise distribution alignment strategy.

Comparison between style prompt and other prompts. As shown in Figure 6, compared to Co-Prompt and CoCo-Prompt

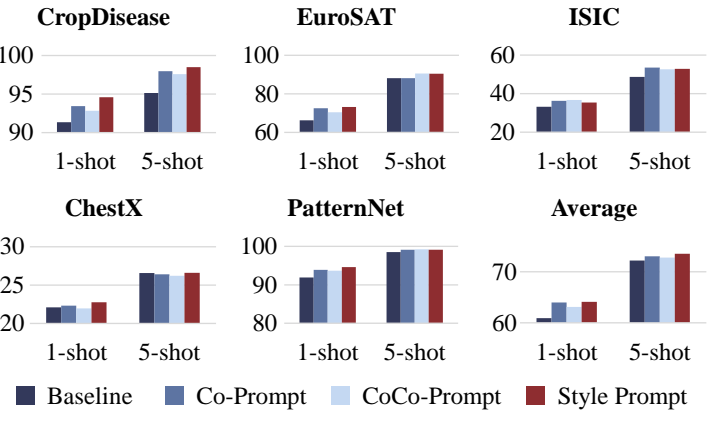


Fig. 6. Comparison of style prompt and the current prompts in 5-way 1-shot and 5-way 5-shot tasks.

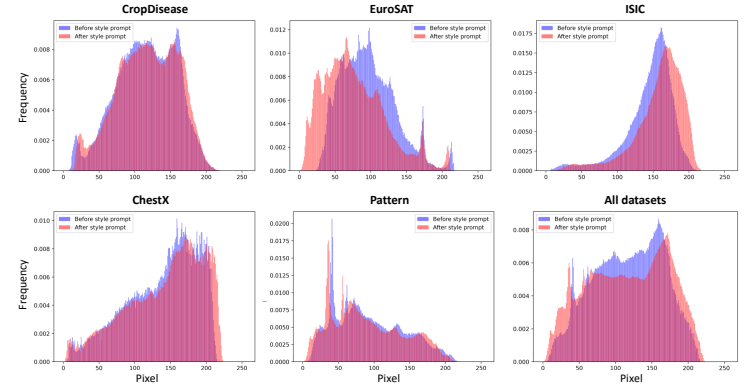


Fig. 7. Histogram differences between data before and after style prompt tuning. Blue part means before style prompt, and red part indicates after style prompt.

(where the style prompt in StepSPT is replaced by text prompts from CoOp and CoCoOp), the proposed style prompt achieves the best average performance. However, Co-Prompt and CoCo-Prompt achieve higher results than the style prompt on ISIC, indicating that, compared to visual prompts, text prompts can better alleviate performance degradation caused by background interference.

Style prompt visualization. This paper modifies image styles by adjusting the statistical characteristics in normalization. Current style transfer methods [68] use a nonlinear decoder to amplify the style effect, which introduces noise [69]. Thus, we use histograms to show statistical characteristics rather than directly visualizing the style transfer. This approach allows us to observe the impact of style prompts on image statistics more directly, without the noise introduced by the nonlinear network. Figure 7 shows the statistical differences in samples before and after applying the style prompt, which shows that the statistical characteristics significantly change after applying the style prompt.

4.4.2 Performance of Step-wise Distribution Alignment

We evaluate the proposed step-wise distribution alignment strategy from the following aspects. First, we demonstrate the performance of this strategy. Then, we choose the hyper-parameters related to this strategy, including step size, credible group, and loss function.

w/ and w/o Step-wise Distribution Alignment. As illustrated in Table 3, ‘*w/o Style*’ indicates StepSPT without the style prompt, *i.e.* using only the step-wise distribution alignment strategy. Compared to ‘Baseline’, ‘*w/o Style*’ significantly

TABLE 4
Performance of different step size E .

K	E	CropDisease	EuroSAT	ISIC	ChestX	PatternNet	Average
1	2	93.60 \pm 0.73	73.28 \pm 0.67	36.07 \pm 0.43	22.23 \pm 0.42	96.64 \pm 0.26	64.36
	5	93.13 \pm 0.24	73.40 \pm 0.47	37.16 \pm 0.69	22.27 \pm 0.52	94.80 \pm 0.15	64.15
	10	94.45 \pm 0.75	73.79 \pm 1.09	36.93 \pm 0.86	22.84 \pm 0.64	96.69 \pm 0.57	64.94
	20	93.00 \pm 0.15	73.53 \pm 0.37	36.00 \pm 0.31	22.20 \pm 0.71	96.62 \pm 0.67	64.27
	50	94.98 \pm 0.15	73.53 \pm 0.46	36.73 \pm 0.82	22.80 \pm 0.76	96.27 \pm 0.69	64.86
	100	95.39\pm0.22	73.83\pm0.80	37.16\pm0.68	23.73\pm0.98	96.44 \pm 0.42	65.31
5	2	96.64 \pm 0.50	89.00 \pm 0.19	50.93 \pm 0.17	25.80 \pm 0.75	99.53\pm0.38	72.38
	5	96.40 \pm 0.15	90.06 \pm 0.67	51.73 \pm 0.28	25.37 \pm 0.25	99.26 \pm 0.67	72.56
	10	98.67\pm0.76	89.63 \pm 0.30	52.05 \pm 0.51	26.80 \pm 0.33	99.40 \pm 0.28	73.31
	20	98.62 \pm 0.89	89.99 \pm 0.17	51.89 \pm 0.80	25.60 \pm 0.53	99.33 \pm 0.47	73.09
	50	97.10 \pm 0.69	90.20 \pm 0.71	52.20 \pm 0.62	27.07 \pm 0.94	99.33 \pm 0.79	73.18
	100	97.11 \pm 0.60	91.07\pm0.73	53.99\pm0.44	27.11\pm0.75	99.24 \pm 0.32	73.70

improves performance. For example, the average results of ‘w/o Style’ are 3.03% (5-way 1-shot) and 0.93% (5-way 5-shot) higher than ‘Baseline’. This indicates that the strategy is more effective in 5-way 1-shot, particularly in distant domain tasks such as ISIC and ChestX. In 5-way 1-shot task, ‘w/o Style’ is 3.54% and 0.65% higher than ‘Baseline’ on ISIC and ChestX, respectively. However, in the 5-way 5-shot task, the strategy does not have a positive effect on these two datasets. Moreover, comparing ‘w/o Step’ and ‘StepSPT’, combining this strategy with the style prompt further enhances performance. This suggests that, although the strategy decreases performance in distant domains in the 5-way 5-shot task, combining it with the style prompt yields a more positive effect (1.11% higher on ISIC and 0.5% higher on ChestX).

Selection of Step Size. In step-wise distribution alignment strategy, the step size should be studied. Table 4 presents the results of different step size. In 5-way 1-shot task, StepSPT obtains the best average result 65.31% when the step size is 100. A step size of 100 achieves the best results on all datasets except PatternNet. Similar to 5-way 1-shot, the size of 100 also performs best on the 5-way 5-shot task, achieving 73.70% optimal average result. Unlike the 5-way 1-shot task, a step size of 5 performs best only in distant domains (91.07% for EuroSAT, 53.99% for ISIC, and 27.11% for ChestX) but not in near domain (third-optimal 97.11% result for CropDisease). It is worth noting that a step size of 100 achieves an optimal result of 91.07% on EuroSAT but the lowest result of 99.24% on PatternNet. Despite this, we select the overall optimal step size of 100.

Credible Group. As written in the paper, we obtain the credible group \mathcal{G} in two ways: entropy-based ranking \mathcal{G}_{en} , and prototype-based ranking \mathcal{G}_{pro} . In Table 5, we demonstrate the effectiveness of each group. Compared to using only \mathcal{G}_{en} or \mathcal{G}_{pro} separately, \mathcal{G} performs best on all 5 datasets (0.56% higher on CropDisease, 0.02% higher on EuroSAT, 3.07% higher on ISIC, 0.22% higher on ChestX, 0.48% higher on PatternNet, and 0.97% higher on average) in 5-way 1-shot task. However, in the 5-way 5-shot task, \mathcal{G} achieves sub-optimal results on CropDisease, EuroSAT, and PatternNet. Specifically, \mathcal{G}_{en} performs best on CropDisease (98.29%), while \mathcal{G}_{pro} achieves the best performance on EuroSAT (91.22%) and PatternNet (99.73%). Therefore, \mathcal{G}_{en} can make up for the performance shortcomings on CropDisease by introducing a small amount of labeled data, while \mathcal{G}_{pro} ’s performance shortcomings in remote sensing also can be compensated by adding more labeled data.

Additionally, the number of selected samples in \mathcal{G}_{en} and \mathcal{G}_{pro} depends on α and γ . Therefore, Figure 8 illustrates the selection of α and γ . For α , we choose from values [0.1, 0.3, 0.5, 0.7, 0.9]. The optimal values of α for all datasets (CropDisease to PatternNet) are 0.9, 0.7, 0.3, 0.5, and 0.9. We observe that α tends to the large value for addressing the near domains (0.9 for CropDisease, 0.7 for EuroSAT, and 0.9 for PatternNet), and

TABLE 5
Performance of different credible group with a ConvNeXt backbone.

K	Group	CropDisease	EuroSAT	ISIC	ChestX	PatternNet	Average
1	\mathcal{G}_{en}	94.27 \pm 0.82	72.00 \pm 0.26	34.09 \pm 0.34	23.51 \pm 0.77	94.80 \pm 0.35	63.73
	\mathcal{G}_{pro}	94.83 \pm 0.41	73.81 \pm 0.65	33.82 \pm 0.28	23.27 \pm 1.10	95.96 \pm 0.81	64.34
	\mathcal{G}	95.39\pm0.22	73.83\pm0.80	37.16\pm0.68	23.73\pm0.98	96.44\pm0.42	65.31
5	\mathcal{G}_{en}	98.29\pm0.53	89.82 \pm 0.44	52.96 \pm 0.34	26.62 \pm 0.66	99.47 \pm 0.32	73.43
	\mathcal{G}_{pro}	96.00 \pm 0.87	91.22\pm0.53	51.24 \pm 0.88	25.29 \pm 0.45	99.73\pm0.29	72.70
	\mathcal{G}	97.11 \pm 0.60	91.07 \pm 0.73	53.99\pm0.44	27.11\pm0.75	99.24 \pm 0.32	73.70

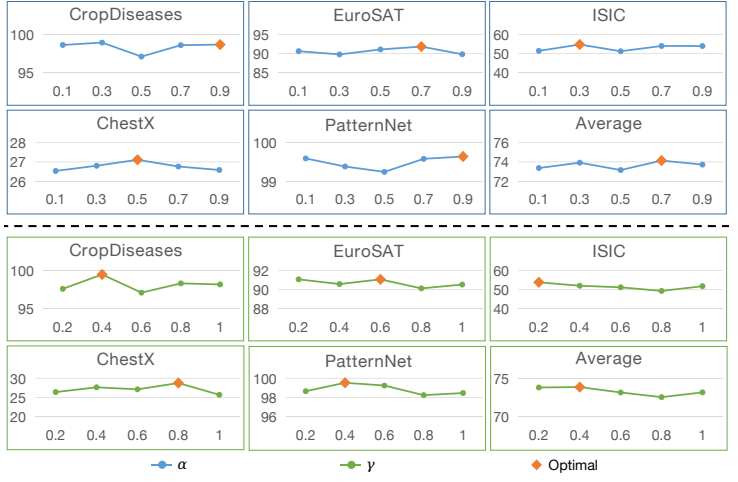


Fig. 8. Results of StepSPT with different α and γ on 5-way 5-shot task. The upper part means the performance of α on different datasets, and the down part is the selection of γ on all datasets.

TABLE 6
Comparison of KL and MI loss effectiveness in 5-way 5-shot task.

Methods	CropDisease	EuroSAT	ISIC	ChestX	PatternNet	Avg
Baseline	95.15 \pm 0.29	88.11 \pm 0.90	52.51 \pm 0.48	26.57 \pm 0.21	98.52 \pm 0.36	72.17
w/o MI	96.49 \pm 0.69	90.64 \pm 0.32	51.38 \pm 0.79	26.18 \pm 0.80	99.69\pm0.32	72.88
w/o KL	96.31 \pm 0.33	90.08 \pm 0.61	53.82 \pm 0.53	26.40 \pm 0.62	99.07 \pm 0.70	73.34
StepSPT	97.11\pm0.60	91.07\pm0.73	53.99\pm0.44	27.11\pm0.75	99.24 \pm 0.32	73.79

the small value for distant domains (0.3 for ISIC and 0.5 for ChestX). This non-uniformity across domains suggests that sub-optimal values (0.7, 0.5, 0.7, 0.3, 0.7) offer a potential for setting α at 0.7. Moreover, the average optimal results of all datasets is 0.7. Therefore, the best selection of α is 0.7. Similarly for γ , we choose from [0.2, 0.4, 0.6, 0.8, 1.0], where the best selections from CropDisease to PatternNet are: 0.4, 0.6, 0.2, 0.8, 0.4. Following the selection of α , we also analyze sub-optimal values of γ across datasets: 0.8, 0.4, 0.4, 0.4, 0.6. And the best average result of γ is 0.4, which guides us to set the optimal result of γ to 0.4. These configurations (0.7 for α and 0.4 for γ) suggest that selecting more top-k samples with lower entropy enhances \mathcal{G} ’s reliability, while decreasing γ improves performance, indicating a preference for fewer topk prototype samples.

Loss Function L_{MI} and L_{KL} . Table 6 highlights the effectiveness of KL and MI loss within the step-wise distribution alignment strategy. As shown in the table, ‘w/o MI’ outperforms ‘Baseline’ in near domains such as CropDisease (96.49% vs. 95.15%), EuroSAT (90.64% vs. 88.11%), and PatternNet (99.69% vs. 98.52%), but underperforms in distant domains like ISIC (51.38% vs. 52.51%) and ChestX (26.18% vs. 26.57%). An analysis suggests that the KL loss considers only sample diversity and ensures that samples are evenly classified into each category. However, it ignores the constraints of distance between data pairs, leading to reduced performance in distant domains. While In contrast, ‘w/o KL’ outperforms ‘Baseline’ across nearly all datasets (96.31% vs. 95.15% for CropDisease, 90.08% vs. 88.11% for EuroSAT, 53.82% vs. 52.51% for ISIC, and 99.07% vs. 98.52% for PatternNet). This

TABLE 7
Performance of Label Propagation (LP) on all 5 datasets in 5-way K -shot task.

K	Backbone	Methods	CropDisease	EuroSAT	ISIC	ChestX	PatternNet	Avg
1	ViT	VPT	75.00 \pm 0.24	67.53 \pm 0.59	30.80 \pm 0.96	20.56 \pm 0.64	79.87 \pm 0.69	54.75
		StepSPT w/o LP	81.00 \pm 0.33	67.35 \pm 0.59	31.01 \pm 0.49	23.06 \pm 0.62	79.63 \pm 0.73	56.41
		StepSPT w/ LP	82.56\pm0.27	68.47\pm0.22	32.03\pm0.42	23.55\pm1.06	80.84\pm0.31	57.49
	CLIP	CoCoOp	75.37 \pm 0.78	71.56\pm0.85	30.07 \pm 0.36	20.23 \pm 0.84	90.55 \pm 0.31	57.56
		StepSPT w/o LP	82.69 \pm 0.64	70.25 \pm 0.31	31.88 \pm 0.83	22.62 \pm 0.28	92.47 \pm 0.57	59.98
		StepSPT w/ LP	84.84\pm0.72	70.01 \pm 0.21	32.97\pm0.27	22.84\pm0.95	95.16\pm0.51	61.16
	ConvNeXt	DARA	91.80 \pm 0.85	69.54 \pm 0.62	34.99 \pm 0.53	22.66 \pm 0.75	93.49 \pm 0.65	62.50
		IM-DCL w/o LP	92.60 \pm 0.50	70.07 \pm 0.60	34.53 \pm 0.97	21.60 \pm 0.97	91.79 \pm 0.44	62.12
		StepSPT w/o LP	92.17 \pm 0.43	70.53 \pm 0.47	34.62 \pm 0.77	23.33 \pm 0.91	92.44 \pm 0.62	62.62
		IM-DCL w/ LP	95.13 \pm 0.95	71.27 \pm 0.42	36.53 \pm 0.93	23.53 \pm 0.26	93.47 \pm 0.57	63.99
		StepSPT w/ LP	95.39\pm0.22	73.83\pm0.80	37.16\pm0.66	23.73\pm0.98	96.44\pm0.42	65.31
		VPT	95.20 \pm 0.99	78.05 \pm 0.39	50.00 \pm 0.44	26.63 \pm 1.03	93.24 \pm 0.74	68.62
5	ViT	StepSPT w/o LP	95.39 \pm 0.49	82.51 \pm 0.24	49.95 \pm 0.36	25.31 \pm 0.84	93.88 \pm 0.66	69.41
		StepSPT w/ LP	97.07\pm0.75	84.88\pm0.28	50.39\pm0.34	26.65\pm0.11	95.96\pm0.65	70.99
		CoCoOp	90.20 \pm 0.34	86.07 \pm 0.62	46.99 \pm 0.71	26.15 \pm 0.83	98.71 \pm 0.40	69.62
	CLIP	StepSPT w/o LP	93.53 \pm 0.37	87.52 \pm 0.29	49.98 \pm 0.14	26.29 \pm 0.59	98.64 \pm 0.81	71.19
		StepSPT w/ LP	96.01\pm0.88	89.40\pm1.05	52.12\pm0.36	26.36\pm0.97	99.04\pm0.31	72.58
		DARA	95.65 \pm 0.25	82.12 \pm 0.26	50.80 \pm 0.86	26.37 \pm 0.51	98.62 \pm 0.37	70.71
	ConvNeXt	IM-DCL w/o LP	96.33 \pm 0.33	82.33 \pm 0.81	50.93 \pm 0.48	27.03 \pm 0.71	98.00 \pm 0.41	70.92
		StepSPT w/o LP	96.53 \pm 0.52	89.20 \pm 0.88	50.62 \pm 0.62	27.06 \pm 0.27	98.71 \pm 0.49	72.42
		IM-DCL w/ LP	97.33\pm0.33	84.53 \pm 0.90	54.33\pm0.37	26.40 \pm 0.98	99.00 \pm 0.42	72.32
		StepSPT w/ LP	97.11 \pm 0.60	91.07\pm0.73	53.99 \pm 0.44	27.11\pm0.75	99.24\pm0.32	73.79

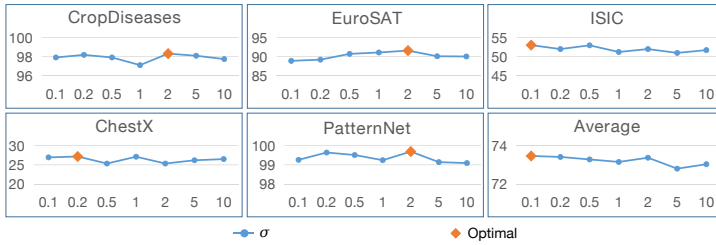


Fig. 9. Results of StepSPT with different σ on all the datasets in 5-way 5-shot task.

improvement is attributed to the MI loss, which reduces the distance between data pairs, resulting in the model being able to classify the sample deterministically even in the distant domain. Additionally, the average performance of ‘w/o KL’ surpasses ‘w/o MI’ (72.88%), suggesting that MI loss is more crucial than KL loss. Moreover, combining MI and KL losses in StepSPT further enhances classification performance, which emphasizes the importance of reducing distances of data pairs and maintaining diversity.

In addition, the hyper-parameter σ is also important for L_{ex} , which controls the strength of the KL loss effect. Figure 9 show the performance of different σ in 5-way 5-shot task. The figure shows that the optimal σ differs between near (CropDisease, EuroSAT, and PatternNet) and distant domains (ISIC and ChestX). Specifically, in near domains, the best performance is achieved (98.31% for CropDisease, 91.56% for EuroSAT, and 99.69% for PatternNet) when σ is set to a high value of 2. While in the distant domains, the optimal set of σ is small like 0.1 or 0.2. For example, the best result on ISIC is 52.98% when $\sigma=0.1$, and the optimal performance on ChestX is 27.16% when σ is 0.2. This suggests that KL loss plays a more limited role in distant domains, so a lower weight is preferred. This coincides with the conclusion obtained in Table 6, where ‘w/o KL’ corresponds to σ set to 0, and ‘w/o MI’ is similar to that σ is set to an infinity constant. Figure 9 further illustrates paying too much attention to KL loss will have a negative effect on distant domain tasks due to ignoring the uncertainty constraints of MI loss. Therefore, σ is set to 2 for near domains and 0.1 for distant domains.

4.5 Performance Analysis

In this section, we focus on the analysis of StepSPT’s performance from three perspectives: (1) introduction of

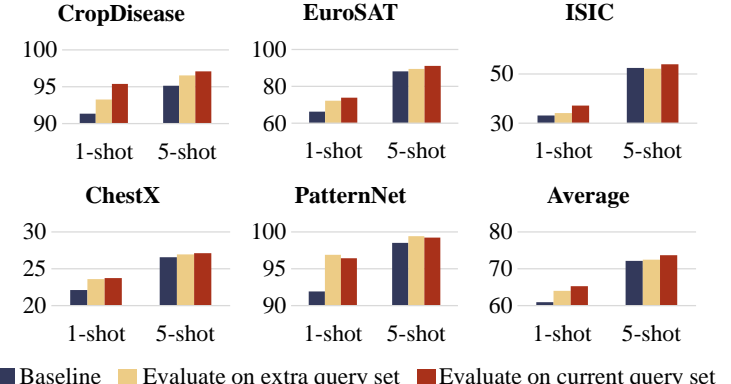


Fig. 10. Evaluate on extra query set on all 5 datasets in both 5-way 1-shot and 5-way 5-shot tasks.

Label Propagation (LP), (2) generalization to the extra query set, and (3) T-SNE visualization of the proposed StepSPT.

4.5.1 Label Propagation (LP)

To further demonstrate the performance of StepSPT, we compare ‘StepSPT w/o LP’ with the current SOTAs, such as VPT, CoCoOp, DARA, and IM-DCL, and ‘StepSPT w/ LP’ on different backbones. The comparison between ‘StepSPT w/o LP’ and SOTAs demonstrates StepSPT’s superior performance, and ‘StepSPT w/ LP’ can further demonstrate the effect of LP, as shown in Table 7. For the ViT backbone, ‘VPT’ outperforms ‘StepSPT w/o LP’ on EuroSAT (0.18% higher) and PatternNet (0.24% higher), indicating that ViT-based StepSPT has limited effectiveness in remote sensing. However, this limitation disappears in the 5-way 5-shot task, where ‘StepSPT w/o LP’ outperforms ‘VPT’ on all datasets (4.46% higher on EuroSAT and 0.64% higher on PatternNet). Additionally, ‘StepSPT w/ LP’ achieves the best results compared to ‘StepSPT w/o LP’ and ‘VPT’. For the CLIP backbone, we compare ‘StepSPT w/o LP’ and ‘StepSPT w/ LP’ with ‘CoCoOp’. Since CLIP is based on ViT, similar to ViT backbone, ‘CoCoOp’ similarly achieves the best performance on EuroSAT (71.56%) in the 5-way 1-shot task, while ‘StepSPT w/o LP’ obtains 70.25%. And same to ViT backbone, this phenomenon disappears as the amount of data increases, i.e. 87.52% of ‘StepSPT w/o LP’ is higher than 86.07% of ‘CoCoOp’ on EuroSAT in the 5-way 5-shot task. And ‘StepSPT w/ LP’ is better than the other two, meaning the effect of LP.

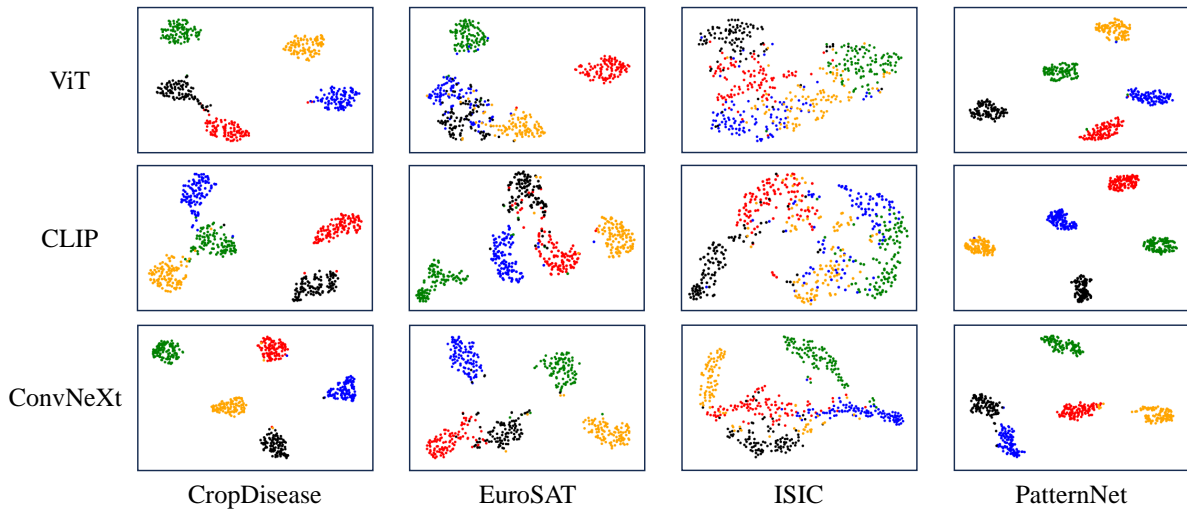


Fig. 11. T-SNE visualization of StepSPT on different backbones: ViT, CLIP, and ConvNeXt.

Moreover, for the ConvNeXt backbone, we first compare ‘StepSPT w/o LP’ with ‘DARA’ and ‘IM-DCL w/o LP’ to demonstrate the superiority of StepSPT. Specifically, ‘StepSPT w/o LP’ outperforms ‘IM-DCL w/o LP’ and ‘DARA’ on almost all datasets. For instance, ‘StepSPT w/o LP’ achieves average scores of 62.62% and 72.42% in the 5-way 1-shot and 5-way 5-shot tasks, respectively, compared to (62.12%, 70.92%) and (62.50%, 70.71%) for the other two. In addition, ‘StepSPT w/ LP’ performs best on average (65.31%, 73.79%) in both 5-way 1-shot and 5-way 5-shot tasks compared to ‘DARA’ (62.50%, 70.71%), ‘StepSPT w/o LP’ (62.62%, 72.42%) and ‘IM-DCL w/ LP’ (63.99%, 72.32%). In general, we draw the following conclusions: (1) StepSPT still achieves the best results even without the introduction of LP, (2) the introduction of LP further improves the classification performance, and (3) StepSPT achieves the best performance among SOTAs that incorporate LP.

4.5.2 Generalize to Extra Query Set

Given that StepSPT introduces the query set into the external process, it is essential to evaluate its performance on the additional query set. The results of StepSPT on the additional query set are shown in Figure 10. From Figure 10 we observe that the extra query set results outperform the baseline, indicating the effectiveness of transductive learning in StepSPT. Additionally, the extra query set results are also close to those of the current query set, with the extra query set even outperforming the current query set on PatternNet, demonstrating StepSPT’s strong generalization ability. Moreover, this trend remains consistent on both 5-way 1-shot and 5-way 5-shot tasks, further indicating the robustness of transductive learning in the proposed method, *i.e.* its positive effect remains stable as the data amount increases.

4.5.3 T-SNE Visualization

Due to the generally low performance on the 5-way 1-shot task, t-SNE [70] visualization cannot effectively show the characteristics of the proposed method, we present the visualization only for the 5-way 5-shot task, as shown in Figure 11. Additionally, we omit the visualization of ChestX due to its low performance. We observe that CropDisease and PatternNet (with high accuracy) show highly aggregated visual features. However, the separation boundaries of EuroSAT and ISIC (with low accuracy) are relatively vague, which means StepSPT does not have strict constraints on the certainty of features, especially on EuroSAT and ISIC. We use the following example of this phenomenon: a sample that belongs to the third category but gets a prediction

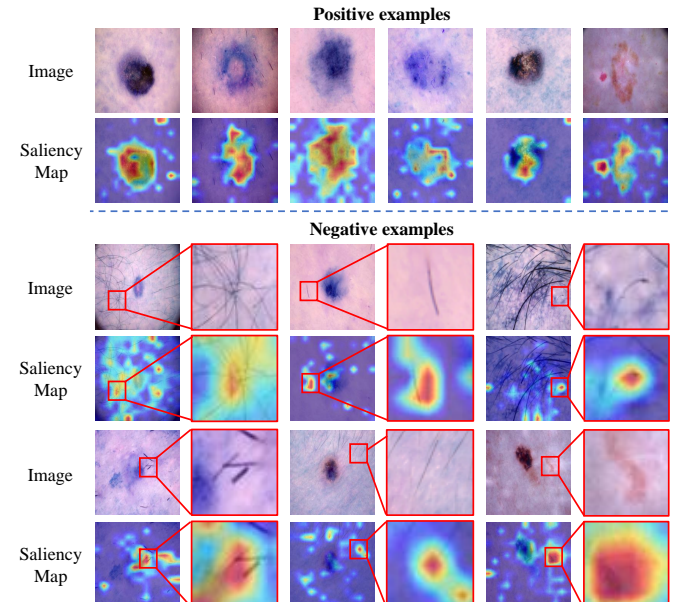


Fig. 12. Positive (correct attention) and negative (incorrect attention) samples on ISIC dataset. The upper row shows the images, and the lower row is the corresponding saliency map to indicate the attention of model.

result of [0.1, 0.31, 0.3, 0.2, 0.1] will be incorrectly classified to the second category. The high uncertainty of these features significantly affects classification accuracy. As discussed in Section 4.3, this phenomenon is attributed to the low resolution of EuroSAT samples and the background interference in ISIC images.

Comparing the visualization of EuroSAT and PatternNet in Figure 11 highlights the importance of resolution, where EuroSAT, compared to PatternNet, shows a tendency towards uncertain classification. As discussed in Section 4.3 for ISIC, the attention of model on ISIC images can easily be distracted by background elements. Figure 12 illustrates examples of correct and incorrect attention [71], where in the error cases, the model focuses on background elements, such as hair.

5 CONCLUSION

This paper introduces Step-wise Distribution Alignment Guided Style Prompt Tuning (StepSPT) to address the source-free cross-domain few-shot learning (SF-CDFSL) problem. StepSPT first proposes a style prompt to quantify and adjust the distribution of target data. It then employs a dual-phase optimization

process, including external and internal processes, to optimize the style prompt. In the external process, a step-wise distribution alignment strategy is proposed while keeping the source model and classifier frozen. In the internal process, the classifier is fine-tuned using cross-entropy loss, with the style prompt and source model remaining fixed. Experimental results on five datasets demonstrate substantial performance enhancements achieved by StepSPT over existing large pretraining models. Ablation experiments further validate the efficacy of the style prompt and the step-wise distribution alignment strategy.

Although StepSPT provides a way to implement SF-CDFSL without fine-tuning LMs, it does not have strict constraints on the certainty of features, especially on EuroSAT and ISIC. The main reason involves the effect of resolution and background. The future work involves addressing the negative impact of such uncertain predictions on accuracy. For example, our future work will involve exploring methods that can effectively handle tasks across multiple resolutions. In addition, to solve the effect of background, giving samples with high uncertainty, called difficult samples, more weight to influence the final loss, making models learn optimal decision boundaries.

REFERENCES

- [1] H. Xu, S. Zhi, S. Sun, V. M. Patel, and L. Liu, "Deep learning for cross-domain few-shot visual recognition: A survey," *arXiv preprint arXiv:2303.08557*, 2023.
- [2] H. Tseng, H. Lee, J. Huang, and M. Yang, "Cross-domain few-shot classification via learned feature-wise transformation," in *ICLR*, 2020.
- [3] C. P. Phoo and B. Hariharan, "Self-training for few-shot transfer across extreme task differences," in *ICLR*, 2020.
- [4] A. Islam, C. R. Chen, R. Panda, L. Karlinsky, R. Feris, and R. J. Radke, "Dynamic distillation network for cross-domain few-shot recognition with unlabeled data," *NeurIPS*, vol. 34, pp. 3584–3595, 2021.
- [5] H. Xu, S. Zhi, and L. Liu, "Cross-domain few-shot classification via inter-source stylization," *ICIP*, 2023.
- [6] Y. Fu, Y. Xie, Y. Fu, and Y. Jiang, "Styleadv: Meta style adversarial training for cross-domain few-shot learning," in *CVPR*, 2023, pp. 24 575–24 584.
- [7] Y. Zhao and N. Cheung, "Fs-ban: Born-again networks for domain generalization few-shot classification," *IEEE TIP*, 2023.
- [8] P. Li, S. Gong, C. Wang, and Y. Fu, "Ranking distance calibration for cross-domain few-shot learning," in *CVPR*, 2022, pp. 9099–9108.
- [9] Y. Zhao, T. Zhang, J. Li, and Y. Tian, "Dual adaptive representation alignment for cross-domain few-shot learning," *IEEE TPAMI*, 2023.
- [10] J. Liang, D. Hu, and J. Feng, "Do we really need to access the source data? source hypothesis transfer for unsupervised domain adaptation," in *ICML*. PMLR, 2020, pp. 6028–6039.
- [11] A. Radford, J. W. Kim, C. Hallacy, A. Ramesh, G. Goh, S. Agarwal, G. Sastry, A. Askell, P. Mishkin, and J. Clark, "Learning transferable visual models from natural language supervision," in *ICML*. PMLR, 2021, pp. 8748–8763.
- [12] A. Dosovitskiy, L. Beyer, A. Kolesnikov, D. Weissenborn, X. Zhai, T. Unterthiner, M. Dehghani, M. Minderer, G. Heigold, and S. Gelly, "An image is worth 16x16 words: Transformers for image recognition at scale," in *ICLR*, 2020.
- [13] B. Liu, Z. Zhao, Z. Li, J. Jiang, Y. Guo, and J. Ye, "Feature transformation ensemble model with batch spectral regularization for cross-domain few-shot classification," *CVPR Challenge*, 2020.
- [14] X. Wang, G. Chen, G. Qian, P. Gao, X.-Y. Wei, Y. Wang, Y. Tian, and W. Gao, "Large-scale multi-modal pre-trained models: A comprehensive survey," *MIR*, vol. 20, no. 4, pp. 447–482, 2023.
- [15] J. Devlin, M.-W. Chang, K. Lee, and K. Toutanova, "Bert: Pre-training of deep bidirectional transformers for language understanding," *arXiv preprint arXiv:1810.04805*, 2018.
- [16] T. Brown, B. Mann, N. Ryder, M. Subbiah, J. D. Kaplan, P. Dhariwal, A. Neelakantan, P. Shyam, G. Sastry, A. Askell *et al.*, "Language models are few-shot learners," *NeurIPS*, vol. 33, pp. 1877–1901, 2020.
- [17] H. Xu, L. Liu, S. Zhi, S. Fu, Z. Su, M.-M. Cheng, and Y. Liu, "Enhancing information maximization with distance-aware contrastive learning for source-free cross-domain few-shot learning," *IEEE TIP*, 2024.
- [18] X. Wang, Y. Peng, L. Lu, Z. Lu, M. Bagheri, and R. M. Summers, "Chestx-ray8: Hospital-scale chest x-ray database and benchmarks on weakly-supervised classification and localization of common thorax diseases," in *CVPR*, 2017, pp. 2097–2106.
- [19] N. Codella, V. Rotemberg, P. Tschandl, M. E. Celebi, S. Dusza, D. Gutman, B. Helba, A. Kalloo, K. Liopyris, and M. Marchetti, "Skin lesion analysis toward melanoma detection 2018: A challenge hosted by the international skin imaging collaboration (isic)," *arXiv preprint arXiv:1902.03368*, 2019.
- [20] W. Li, W. Yang, T. Liu, Y. Hou, Y. Li, Z. Liu, Y. Liu, and L. Liu, "Predicting gradient is better: Exploring self-supervised learning for sar atr with a joint-embedding predictive architecture," *ISPRS JPRS*, vol. 218, pp. 326–338, 2024.
- [21] J. Zhou, C. Xiao, B. Peng, Z. Liu, L. Liu, Y. Liu, and X. Li, "Diffdet4sar: Diffusion-based aircraft target detection network for sar images," *IEEE GRSL*, 2024.
- [22] J. Li, Z. Yu, Z. Du, L. Zhu, and H. T. Shen, "A comprehensive survey on source-free domain adaptation," *IEEE TPAMI*, 2024.
- [23] M. Yazdanpanah and P. Moradi, "Visual domain bridge: A source-free domain adaptation for cross-domain few-shot learning," in *CVPR*, 2022, pp. 2868–2877.
- [24] A. Kumar, T. Ma, and P. Liang, "Understanding self-training for gradual domain adaptation," in *ICML*. PMLR, 2020, pp. 5468–5479.
- [25] S. Tang, A. Chang, F. Zhang, X. Zhu, M. Ye, and C. Zhang, "Source-free domain adaptation via target prediction distribution searching," *IJCV*, pp. 1–19, 2023.
- [26] Y. Guo, N. C. Codella, L. Karlinsky, J. V. Codella, J. R. Smith, K. Saenko, T. Rosing, and R. Feris, "A broader study of cross-domain few-shot learning," in *ECCV*. Springer, 2020, pp. 124–141.
- [27] J. Sun, S. Lapuschkin, W. Samek, Y. Zhao, N. Cheung, and A. Binder, "Explanation-guided training for cross-domain few-shot classification," in *ICPR*. IEEE, 2021, pp. 7609–7616.
- [28] Y. Fu, Y. Fu, and Y. Jiang, "Meta-fdmixup: Cross-domain few-shot learning guided by labeled target data," in *ACM MM*, 2021, pp. 5326–5334.
- [29] Y. Fu, Y. Fu, J. Chen, and Y. Jiang, "Generalized meta-fdmixup: Cross-domain few-shot learning guided by labeled target data," *IEEE TIP*, vol. 31, pp. 7078–7090, 2022.
- [30] Y. Fu, Y. Xie, Y. Fu, J. Chen, and Y. Jiang, "Wave-san: Wavelet based style augmentation network for cross-domain few-shot learning," *arXiv preprint arXiv:2203.07656*, 2022.
- [31] J. Zhang, J. Song, L. Gao, and H. Shen, "Free-lunch for cross-domain few-shot learning: Style-aware episodic training with robust contrastive learning," in *ACM MM*, 2022, pp. 2586–2594.
- [32] Y. Zhang, W. Li, M. Zhang, S. Wang, R. Tao, and Q. Du, "Graph information aggregation cross-domain few-shot learning for hyperspectral image classification," *IEEE TNNLS*, pp. 1–14, 2022.
- [33] S. Roy, M. Trapp, A. Pilzer, J. Kannala, N. Sebe, E. Ricci, and A. Solin, "Uncertainty-guided source-free domain adaptation," in *ECCV*. Springer, 2022, pp. 537–555.
- [34] S. Yang, J. van de Weijer, L. Herranz, and S. Jui, "Exploiting the intrinsic neighborhood structure for source-free domain adaptation," *NeurIPS*, vol. 34, pp. 29 393–29 405, 2021.
- [35] F. Wang, Z. Han, Y. Gong, and Y. Yin, "Exploring domain-invariant parameters for source free domain adaptation," in *CVPR*, June 2022, pp. 7151–7160.
- [36] Y. Zhang, Z. Wang, and W. He, "Class relationship embedded learning for source-free unsupervised domain adaptation," in *CVPR*, June 2023, pp. 7619–7629.
- [37] S. Yang, Y. Wang, K. Wang, and S. Jui, "Attracting and dispersing: A simple approach for source-free domain adaptation," in *NeurIPS*, 2022.
- [38] L. Zhou, N. Li, M. Ye, X. Zhu, and S. Tang, "Source-free domain adaptation with class prototype discovery," *PR*, vol. 145, p. 109974, 2024.
- [39] S. Tang, W. Su, M. Ye, and X. Zhu, "Source-free domain adaptation with frozen multimodal foundation model," in *CVPR*, June 2024, pp. 23 711–23 720.
- [40] M. Jia, L. Tang, B. Chen, C. Cardie, S. Belongie, B. Hariharan, and S. Lim, "Visual prompt tuning," in *ECCV*. Springer, 2022, pp. 709–727.
- [41] K. Zhou, J. Yang, C. C. Loy, and Z. Liu, "Learning to prompt for vision-language models," *IJCV*, vol. 130, no. 9, pp. 2337–2348, 2022.
- [42] K. Zhou, J. Yang, C. Loy, and Z. Liu, "Conditional prompt learning for vision-language models," in *CVPR*, 2022, pp. 16 816–16 825.
- [43] C. Ge, R. Huang, M. Xie, Z. Lai, S. Song, S. Li, and G. Huang, "Domain adaptation via prompt learning," *IEEE TNNLS*, 2023.
- [44] B. Zhu, Y. Niu, Y. Han, Y. Wu, and H. Zhang, "Prompt-aligned gradient for prompt tuning," in *ICCV*, 2023, pp. 15 659–15 669.
- [45] Y. Xin, J. Du, Q. Wang, K. Yan, and S. Ding, "Mmap: Multi-modal alignment prompt for cross-domain multi-task learning," in *AAAI*, vol. 38, no. 14, 2024, pp. 16 076–16 084.
- [46] T. Ma, Y. Sun, Z. Yang, and Y. Yang, "Prod: Prompting-to-disentangle domain knowledge for cross-domain few-shot image classification," in *CVPR*, 2023, pp. 19 754–19 763.
- [47] J. Wu, X. Liu, X. Yin, T. Zhang, and Y. Zhang, "Task-adaptive prompted transformer for cross-domain few-shot learning," in *AAAI*, vol. 38, no. 6, 2024, pp. 6012–6020.

- [48] B. Lester, R. Al-Rfou, and N. Constant, "The power of scale for parameter-efficient prompt tuning," in *ACL*, Nov. 2021.
- [49] P. Liu, W. Yuan, J. Fu, Z. Jiang, H. Hayashi, and G. Neubig, "Pre-train, prompt, and predict: A systematic survey of prompting methods in natural language processing," *ACM CSUR*, 2023.
- [50] Y. Wang, Q. Yao, J. T. Kwok, and L. M. Ni, "Generalizing from a few examples: A survey on few-shot learning," *ACM CSUR*, vol. 53, no. 3, pp. 1–34, 2020.
- [51] S. Abnar, R. v. d. Berg, G. Ghiasi, M. Dehghani, N. Kalchbrenner, and H. Sedghi, "Gradual domain adaptation in the wild: When intermediate distributions are absent," *arXiv preprint arXiv:2106.06080*, 2021.
- [52] J. Shen, Y. Qu, W. Zhang, and Y. Yu, "Wasserstein distance guided representation learning for domain adaptation," in *AAAI*, vol. 32, no. 1, 2018.
- [53] Y. Liu, W. Zhang, and J. Wang, "Source-free domain adaptation for semantic segmentation," in *CVPR*, 2021, pp. 1215–1224.
- [54] S. Yang, Y. Wang, J. Van De Weijer, L. Herranz, and S. Jui, "Unsupervised domain adaptation without source data by casting a bait," *arXiv preprint arXiv:2010.12427*, vol. 1, no. 2, p. 5, 2020.
- [55] J. Snell, K. Swersky, and R. Zemel, "Prototypical networks for few-shot learning," *NeurIPS*, vol. 30, 2017.
- [56] M. Boudiaf, J. Rony, I. M. Ziko, E. Granger, M. Pedersoli, P. Piantanida, and I. B. Ayed, "A unifying mutual information view of metric learning: cross-entropy vs. pairwise losses," in *ECCV*. Springer, 2020, pp. 548–564.
- [57] L. Paninski, "Estimation of entropy and mutual information," *Neural computation*, vol. 15, no. 6, pp. 1191–1253, 2003.
- [58] X. Ji, J. F. Henriques, and A. Vedaldi, "Invariant information clustering for unsupervised image classification and segmentation," in *ICCV*, 2019, pp. 9865–9874.
- [59] M. Jabi, M. Pedersoli, A. Mitiche, and I. B. Ayed, "Deep clustering: On the link between discriminative models and k-means," *IEEE TPAMI*, vol. 43, no. 6, pp. 1887–1896, 2019.
- [60] W. Zhou, S. Newsam, C. Li, and Z. Shao, "Patternnet: A benchmark dataset for performance evaluation of remote sensing image retrieval," *ISPRS journal of photogrammetry and remote sensing*, vol. 145, pp. 197–209, 2018.
- [61] Z. Liu, H. Mao, C.-Y. Wu, C. Feichtenhofer, T. Darrell, and S. Xie, "A convnet for the 2020s," in *CVPR*, 2022, pp. 11 976–11 986.
- [62] Z. Su, J. Zhang, T. Liu, Z. Liu, S. Zhang, M. Pietikäinen, and L. Liu, "Boosting convolutional neural networks with middle spectrum grouped convolution," *IEEE TNNLS*, 2024.
- [63] F. Zhou, P. Wang, L. Zhang, W. Wei, and Y. Zhang, "Revisiting prototypical network for cross domain few-shot learning," in *CVPR*, 2023, pp. 20 061–20 070.
- [64] P. Li, F. Liu, L. Jiao, S. Li, L. Li, X. Liu, and X. Huang, "Knowledge transduction for cross-domain few-shot learning," *PR*, vol. 141, p. 109652, 2023.
- [65] J. Oh, S. Kim, N. Ho, J. Kim, H. Song, and S. Yun, "Refine: Re-randomization before fine-tuning for cross-domain few-shot learning," in *ACM CIKM*, 2022, pp. 4359–4363.
- [66] H. Zheng, R. Wang, J. Liu, and A. Kanezaki, "Cross-level distillation and feature denoising for cross-domain few-shot classification," in *ICLR*, 2023.
- [67] D. Das, S. Yun, and F. Porikli, "Confess: A framework for single source cross-domain few-shot learning," in *ICLR*, 2022.
- [68] X. Huang and S. Belongie, "Arbitrary style transfer in real-time with adaptive instance normalization," in *ICCV*, 2017, pp. 1501–1510.
- [69] L. A. Gatys, A. S. Ecker, and M. Bethge, "Image style transfer using convolutional neural networks," in *CVPR*, 2016, pp. 2414–2423.
- [70] L. Van der Maaten and G. Hinton, "Visualizing data using t-sne." *MLR*, vol. 9, no. 11, 2008.
- [71] J. Adebayo, J. Gilmer, M. Muelly, I. Goodfellow, M. Hardt, and B. Kim, "Sanity checks for saliency maps," *NeurIPS*, vol. 31, 2018.